Journal of Molecular Structure 1360 (2026) 145611

Contents lists available at ScienceDirect

Journal of Molecular Structure

journal homepage: www.elsevier.com/locate/molstr

Structure-guided design and synthesis of selective butyrylcholinesterase inhibitors

Christine Shing Wei Law [a,1], Zhe Ying Ha [a,1], Xavier Brazzolotto [b], Keng Yoon Yeong [a,*]

[a] School of Science, Monash University Malaysia, Jalan Lagoon Selatan, Bandar Sunway, 47500, Selangor, Malaysia
[b] Département de Toxicologie et Risques Chimiques, Institut de Recherche Biomédicale des Armées, 1 Avenue du Général Valérie André, 91220, Brétigny-sur-Orge, France

ARTICLE INFO

Keywords:
Alzheimer's disease
Benzimidazole
Butyrylcholinesterase
Crystal structure
Selective inhibitor

ABSTRACT

Alzheimer's disease (AD) is a progressive neurodegenerative disorder marked by cognitive and non-cognitive decline. Cholinesterase inhibitors remain among the few available treatments, acting by preventing the hydrolysis of acetylcholine to alleviate cholinergic deficits. As butyrylcholinesterase (BChE) activity progressively increases in advanced AD while acetylcholinesterase activity declines, selective BChE inhibition has emerged as a promising therapeutic approach. Benzimidazole is a versatile pharmacophore with diverse biological activities, including cholinesterase inhibition. This study aimed to develop more potent benzimidazole-based cholinesterase inhibitors by modifying the 1- and 2-positions of the benzimidazole core. Among the synthesized compounds, **5IIa** exhibited the most potent selective BChE inhibition at a low micromolar level (IC_{50} = 0.4 μM). Human BChE (*h*BChE) was co-crystallized with **5IIa** to resolve the structure of the protein–ligand complex by X-ray crystallography. Owing to its labile nature, **5IIa** was subsequently modified to yield a series of derivatives (**5IIa1**–**7**), which demonstrated potent and selective inhibition of equine BChE (*eq*BChE), with IC_{50} values ranging from 1.07 to 7.86 μM. Lead compound **5IIa6** inhibited *h*BChE with an IC_{50} of 5.9 μM and was identified as a mixed-mode inhibitor based on kinetic studies. **5IIa6** was also predicted to have high blood-brain barrier permeability in an *in vitro* model, while cell viability assay against neuroblastoma and microglial cells indicated no significant toxicity. Taken together, these findings identify **5IIa6** as a promising and selective BChE inhibitor that warrants further investigation as a potential therapeutic agent for AD.

1. Introduction

Alzheimer's disease (AD) is a chronic and progressive neurodegenerative disorder that primarily affects individuals over the age of 60. As the most common form of dementia, AD accounts for more than two-thirds of the 55 million dementia cases worldwide [1–4] Moreover, with increasing life expectancy, its prevalence is projected to triple by 2050 [1–3] Clinically, AD is characterized by a gradual and irreversible decline in cognitive and non-cognitive functions. Cognitive impairment manifests as progressive memory loss, language deterioration, and impaired judgment. At the same time, non-cognitive symptoms include behavioral and personality changes such as delusions, agitation, depression, and loss of social functioning [5,6].

The pathology of AD arises from complex biochemical disturbances in the brain, notably cholinergic dysfunction, amyloid-β plaque deposition, and tau hyperphosphorylation [7] Among these, the cholinergic hypothesis, one of the earliest and most widely studied theories, attributes early AD pathogenesis to a marked loss of cholinergic neurons and a subsequent decline in acetylcholine (ACh) levels [8–10] ACh is the key excitatory neurotransmitter involved in learning, memory, and attention [11–13] ACh deficiency as a result of neuronal loss and reduced activity of choline acetyltransferase (ChAT), disrupts synaptic neurotransmission and eventually leads to cognitive and non-cognitive dysfunctions of the disease [11] Therefore, the cholinergic system remains a rational pharmacological target in AD drug discovery [14,15].

Currently, three of the four FDA-approved symptomatic AD treatments are cholinesterase (ChE) inhibitors that act by inhibiting ChE, the enzyme responsible for hydrolyzing ACh, thereby increasing synaptic ACh levels [16,17] As ACh hydrolysis is inhibited, enhanced ACh availability leads to sustained activation of cholinergic receptors, improved neurotransmission, and partial restoration of cognitive and neuronal functions [8,17–19] Among them, donepezil and galantamine

* Corresponding author.
E-mail address: yeong.kengyoon@monash.edu (K.Y. Yeong).
[1] Contributed equally to this work and should be considered as shared first author.

https://doi.org/10.1016/j.molstruc.2026.145611
Received 17 October 2025; Received in revised form 14 January 2026; Accepted 7 February 2026
Available online 9 February 2026

are selective acetylcholinesterase (AChE) inhibitors, whereas rivastigmine acts as a dual inhibitor, inhibiting both AChE and butyrylcholinesterase (BChE).

For the past few decades, the predominant therapeutic strategy for slowing AD neurodegeneration has been to enhance brain ACh levels by inhibiting AChE [20,21] However, AChE inhibitors provide only modest clinical benefits [16,22] Their limited efficacy, along with frequent adverse effects, underscores the pressing need for improved therapeutic options in AD management [23] AChE has been estimated to account for approximately 95 % of the overall ChE activity in the healthy human brain [14] Studies comparing brain tissues from healthy controls and AD patients revealed marked shifts in ChE activity. AChE levels in the cortex and hippocampus declined by up to 33 % and 38 %, respectively, whereas BChE levels rose by 40 % and 65 %. These changes could be attributed to the loss of AChE-rich cholinergic synapses and neurons, accompanied by an increase in BChE-rich glial cells. The increasing importance of BChE as the disease progresses suggests that it may surpass AChE as the key ChE target in advanced AD [14,24].

Evidence from multiple studies using AChE-knockout mice has supported the contribution of BChE to ACh hydrolysis. AChE-deprived mice were able to survive to adulthood with normal levels of BChE, indicating that BChE is capable of compensating for the role AChE has in cholinergic neurotransmission [14,25] Moreover, selective BChE inhibition has been shown to enhance cognitive performance in aged rats, while similar treatment in transgenic AD mice reduced amyloid-β peptide levels [26,27] Together, these findings suggest that targeting BChE could simultaneously address two major pathological mechanisms in AD, ACh hydrolysis and amyloid-β fibrillization, thereby offering a dual therapeutic benefit.

Given the pivotal role of BChE in advanced stages of AD, the development of selective BChE inhibitors represents a promising therapeutic strategy. However, no BChE-targeted drugs have yet reached the market. In this study, the benzimidazole scaffold was employed as the core structure for the design of novel compounds. This pharmacophore has attracted considerable attention in medicinal chemistry due to its diverse pharmacological activities, including anti-microbial, anti-inflammatory, anti-oxidant, anti-obesity, anti-cancer, anti-tuberculosis, and anti-ChE activities [28–37] Benzimidazoles have been widely investigated, with several derivatives reported as ChE inhibitors with potential utility in AD therapy [38–40].

Although benzimidazole derivatives have been previously reported as anti-ChE agents, a systematic exploration of their structural modifications remains limited [38,41,42] Substitutions at the 1- and 2-positions of the benzimidazole scaffold are known to influence biological activity, yet their impact on ChE inhibition has not been fully elucidated. In pursuit of more potent benzimidazole-based ChE inhibitors, we report herein the design, synthesis, and ChE inhibitory activity of compounds bearing different substituents at the 1- and 2-positions of the benzimidazole core (R^1 and R^2 positions in Fig. 1). The structure-activity relationships (SAR) were assessed through *in vitro* ChE assays and further drug design exploration was aided by protein-ligand crystal structure analysis. Additional studies on cytotoxicity and blood-brain barrier (BBB) permeability of the compounds were also conducted.

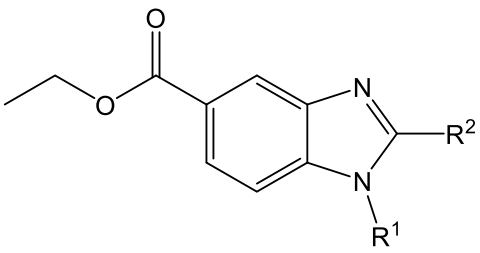

Fig. 1. Benzimidazole scaffold bearing different substituents at the R^1 and R^2 positions.

2. Results and discussion

2.1. Synthesis of benzimidazole derivatives

Benzimidazoles have been reported to show good ChE inhibition with various substitutions at the 2-position [37,40] Specifically, previous studies from our group have also shown that certain compounds containing the ethyl carboxylate and phenyl motifs at the 5-position and 2-position, respectively, gave potent ChE inhibitory activities [28,43] Following that, as the use of different starting materials allows for a wide range of chemical modifications on the benzimidazole nucleus, we further investigated structural changes on cholinesterase inhibitory activities at the 1-position and 2-position in this study.

The benzimidazoles in this study were obtained through a 4-step synthesis involving esterification, amine alkylation, nitro group reduction, and a final condensation reaction (Fig. 2). Fischer esterification of 4-fluoro-3-nitrobenzoic acid with concentrated sulfuric acid by reflux in ethanol yielded the ethyl benzoate **1**. The ethyl benzoate **1** was stirred overnight in dichloromethane (DCM) at 60 °C with the R^1 amine **I**, while for R^1 amine **II**, room temperature was sufficient with the addition of Hünig's base (*N,N*-diisopropylethylamine, DIPEA). The amino product **2** was then reduced *via* 10 % Pd/C and ammonium formate to yield a phenylenediamine intermediate **3**. This intermediate **3** was immediately refluxed overnight with the sodium bisulfite adduct bearing the R^2 moiety of interest in dimethylformamide (DMF). The diamine (with both nitrogen-containing groups ortho to each other) is essential for the formation of the benzimidazole core structure, while the other reagent can be a carboxylic acid, esters, acyl chloride, nitriles, ketones, or aldehyde [44,45] The sodium metabisulfite method was chosen as it was environmentally friendly and cost-efficient. The general protocol was modified from Yeong *et al.* This methodology was applied to the synthesis of two series of ethyl-(1,2-disubstituted)-5-carboxylate benzimidazole derivatives [28,31,46].

The series differ by the R^1 group substituted at the 1-position, whereby **I**: phenyl and **II**: 1-propyl-2-pyrrolidinone. Different R^2 substituents (**a**–**f**) at the 2-position allow SAR studies. According to Chiou et al., *para*-substitution on the phenyl group is preferred for ChE inhibitors, which led to the preparation of **5Ia**–**f** and **5IIa**–**f** [47] Further modification for bioactivity testing led to the synthesis of **5IIg**–**l**. These benzimidazole compounds were then assayed for ChE inhibitory activity.

2.2. Cholinesterase inhibitory activity of synthesized compounds

From preliminary screening of the benzimidazole derivatives at 10 μM, the unsubstituted phenyl R^2 moiety, **a**, displayed high *eq*BChE inhibition in both **5I** and **5II** series, suggesting the R^2 moiety played a greater role in binding with *eq*BChE. **5Ia** exhibited 78.43 % inhibition on *eq*BChE, significantly higher than all the other compounds in the **5I** series (Table 1). With the 1-propyl-2-pyrrolidinone, **5IIa** had a complete inhibition against *eq*BChE, (> 99 %)– the highest recorded in this study, suggesting a potential hit compound (Table 1).

There was no observable trend in ChE inhibition at the *para*-substitution on the R^2 phenyl group, as substitution with electron-donating and -withdrawing groups both showed weaker activity compared to the non-substituted compound **a**. This suggests the steric effect of the substitution may outweigh the electronic effect in rendering activity. None of the compounds displayed an inhibition for *ee*AChE that could rival that of donepezil, the potent *ee*AChE-selective inhibitor. Meanwhile, two compounds (**5Ia** and **5IIa**) were found to have greater *eq*BChE inhibition than galantamine, a dual ChE inhibitor. The significance of the 1-propyl-2-pyrrolidinone, **II**, was evident from the highest ChE inhibition displayed by **5IIa**. As such, an additional six benzimidazole derivatives (**5IIg**–**l**) with different R^2 substitutions were synthesized for evaluation. Heterocyclic groups were included at this stage to evaluate if different functional groups and increased steric bulk at the R^2 position

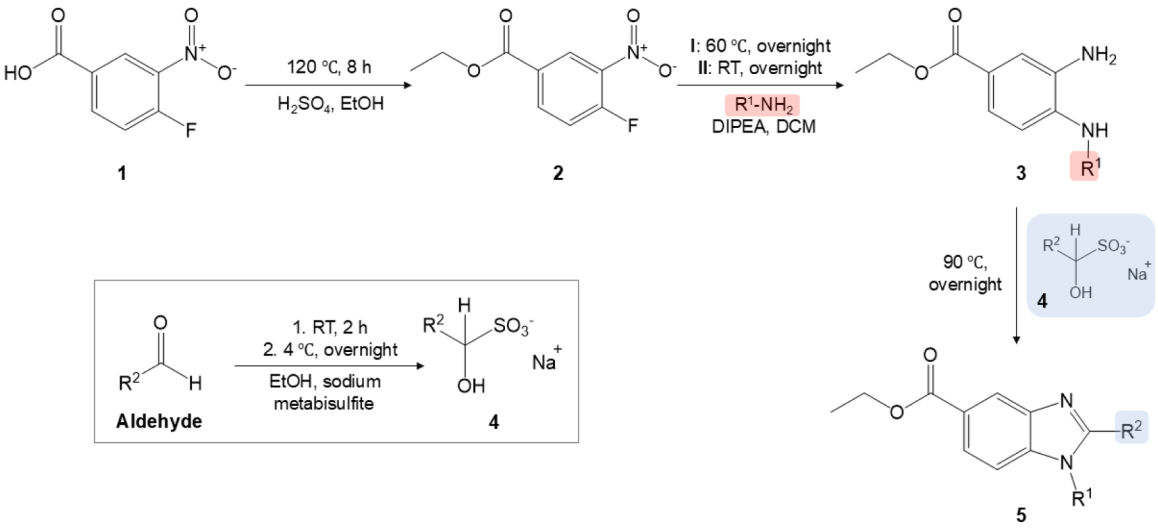

Fig. 2. Reaction pathway to synthesize the final 2-substituted benzimidazole derivatives.

would improve the results. However, no improvement in ChE inhibition was observed upon further modifications at the R^2 position, suggesting steric hindrance to be a possible factor, as initially suspected.

Overall, the unsubstituted phenyl moiety, **a**, was shown to have good *eq*BChE inhibitory properties in both **5I** and **5II** series, with **5IIa** (*eq*BChE IC_{50} = 0.40 μM) exhibiting 4.7-fold increase in potency than **5Ia** (*eq*BChE IC_{50} = 1.88 μM). **5IIa** was found to be selective against *eq*BChE, with a selectivity of over 13-fold over *ee*AChE (*ee*AChE IC_{50} = 5.53 μM, *eq*BChE IC_{50} = 0.40 μM). Through this initial screening, it was established that the combination of 1-propyl-2-pyrrolidinone, **II**, and the phenyl moiety, **a**, provided the most promising *eq*BChE inhibitor and thus was chosen as the scaffold for further modification.

2.3. Structural analysis of the 5IIa binding mode into human BChE

To initiate the **5IIa** structural study in BChE, molecular docking was conducted using Boltz-2, a deep-learning model that predicts accurate biomolecular complex structures as no experimental structure of *eq*BChE is currently available[48] Predictions were conducted for both *eq*BChE, used above for inhibition assays, and *h*BChE, the only BChE that allows X-ray crystallization studies, to date (see below). Interestingly, the predicted complex structures display discrepancies depending on the BChE considered (Fig. 3). The oxopyrrolidine ring sits above Trp82 in both enzymes, but the benzimidazole ring and its respective substituents, benzyl and ester moieties, adopt different orientations, with the benzyl ring fits into the active site gorge for *h*BChE, while it points out of the enzyme for *eq*BChE. A discrepancy between these two enzymes, both in their affinities for different inhibitors[49,50] and in their respective dynamics, as assessed by molecular dynamics studies, especially at the acyl-loop (residues 280–290)[51] has been previously reported.

To further study **5IIa**, human BChE (*h*BChE) was co-crystallized in the presence of the compound to determine the structure of the protein-ligand complex by X-ray crystallography (Fig. 4 and Table 2). In contrast to previously determined structures of *h*BChE in complex with aromatic groups, the main interaction does not involve Trp231. Instead, the present structure reveals interactions with the catalytic histidine residue (His438) and Trp82, the latter of which is involved in a cation-π interaction with choline-based substrates. This could be one of the reasons why we only observed moderate inhibitory activity against *h*BChE (12 uM). Interestingly, the determined crystal structure is close to the Boltz-2-predicted complex, demonstrating the robustness of this deep-learning-based prediction tool. The phenyl group of **5IIa** engages in π-π interactions with both His438 and Trp82 rings, with respective ring-ring distances of 5.4 and 5.2 Å. Interestingly, the sp^2 oxygen atom of the oxopyrrolidine ring engages in a strong intramolecular interaction with the **5IIa** phenyl group, characterized by an atom-ring distance of 3.2 Å. The nitrogen atom of the benzimidazole ring is too far for efficient H-bonding (3.9 Å) with the water molecule present in the oxyanion hole. Here, the water molecule interacts with the nitrogen atoms of Gly116 and Gly117, as well as the O_γ atom of Ser198, at distances of 3.3, 2.8, and 2.6 Å, respectively. Similarly, the benzimidazole ring is too far from the Tyr332 ring, forming the peripheral aromatic site with Asp70, for efficient π-π interaction (7.4 Å). The oxopyrrolidine ring sits in a hydrophobic pocket above Trp82, while the ester moiety is partly pointing out into the solvent.

2.4. Structural modification of 5IIa

Compound **5IIa** was further structurally modified according to the profile presented in Fig. 5. The ethyl ester side chain of **5IIa** was extended to a propyl ester in **5IIa1**. Consistent with this approach, Radzyminska-Lenarcik and Witt reported increased stability constants with longer alkyl chains [52] Second, **5IIa2** and **5IIa3** were designed as secondary and tertiary esters, respectively, since increasing substitution on the ester center can further slow hydrolysis [53] In addition, the labile ester linkage was replaced with an amide, a modification known to confer resonance stabilization and improved hydrolytic resistance. This substitution has been reported to enhance oral bioavailability by up to 22-fold compared to the corresponding ester [53–55] Accordingly, the ester in **5IIa** was converted to an amide in **5IIa4**, which was further modified into **5IIa5** and **5IIa6** by substituting the propyl side chain in **5IIa4** with a phenyl or cyclohexane group, respectively. Aromatic substituents provide resonance stabilization and lower reactivity, whereas cyclohexane introduces rigidity and steric hindrance, both of which can enhance metabolic stability [56] Finally, **5IIa7** was prepared to investigate the substitution effect at the 6-position of the benzimidazole scaffold. All novel derivatives were synthesized *via* multistep procedures (Fig. 6), purified, and subsequently evaluated for their ChE inhibitory activities.

2.5. Cholinesterase inhibitory activity of modified compounds

The modified compounds were assessed for their inhibitory activity against *eq*BChE and *ee*AChE (Table 3). All compounds displayed micromolar potency toward *eq*BChE, with **5IIa2** (secondary ester) and **5IIa1** (primary ester) emerging as the most potent inhibitors (IC_{50} = 1.07 and 1.4 μM, respectively). Meanwhile, **5IIa7**, showed marginally

Table 1
Inhibitory activity and IC_{50} of benzimidazole compounds against *ee*AChE and *eq*BChE.

Compound	Structure	*ee*AChE inhibition ± SD @ 10 μM (%)	*eq*BChE inhibition ± SD @ 10 μM (%)	*ee*AChE IC_{50} ± SD (μM)	*eq*BChE IC_{50} ± SD (μM)
5Ia [31]	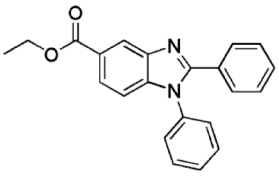	44.27 ± 0.66	78.43 ± 11.17	-	1.88 ± 0.27
5Ib [31]	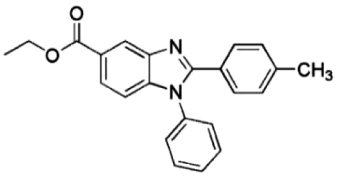	20.44 ± 3.86	52.21 ± 3.61	-	-
5Ic [31]	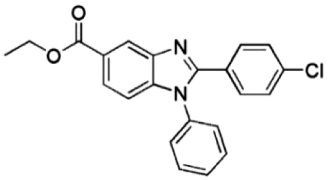	42.45 ± 4.50	23.36 ± 1.63	-	-
5Id [31]	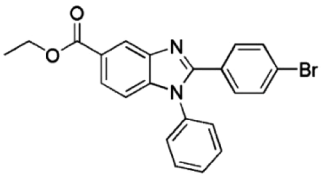	45.11 ± 4.73	37.70 ± 4.79	-	-
5Ie [31]	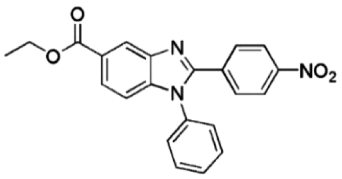	29.85 ± 0.68	37.83 ± 2.93	-	-
5If [31]	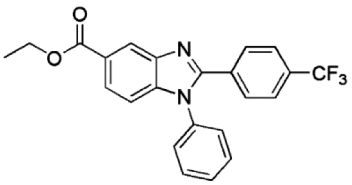	41.50 ± 3.87	39.51 ± 3.20	-	-
5IIa [31,46]	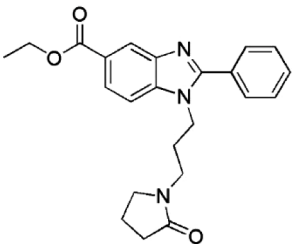	41.38 ± 2.86	> 99 (total inhibition)	5.53 ± 0.96	0.40 ± 0.03

(*continued on next page*)

Table 1 (*continued*)

Compound	Structure	*ee*AChE inhibition ± SD @ 10 μM (%)	*eq*BChE inhibition ± SD @ 10 μM (%)	*ee*AChE IC_{50} ± SD (μM)	*eq*BChE IC_{50} ± SD (μM)
5IIb [31,46]	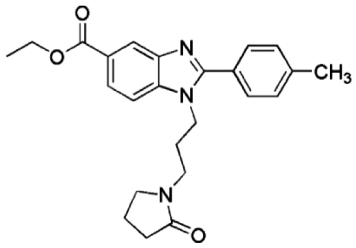	15.06 ± 0.13	39.52 ± 2.16	-	-
5IIc [31]	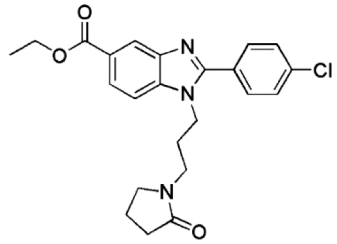	22.09 ± 6.48	27.01 ± 2.07	-	-
5IId [31,46]	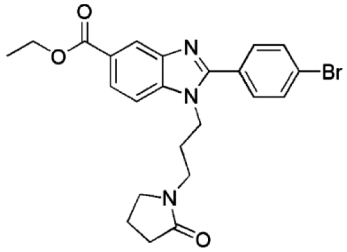	19.33 ± 0.63	17.38 ± 2.29	-	-
5IIe [31,46]	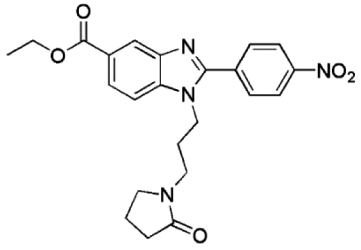	26.64 ± 4.78	25.22 ± 3.20	-	-
5IIf [31,46]	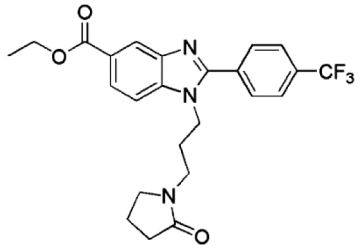	11.40 ± 3.54	18.41 ± 0.32	-	-
5IIg [31,46]	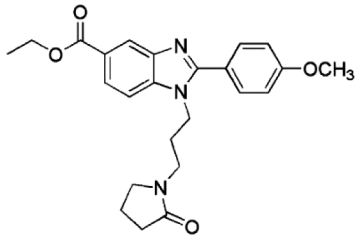	26.10 ± 5.69	42.59 ± 0.99	-	-

(*continued on next page*)

Table 1 (*continued*)

Compound	Structure	*ee*AChE inhibition ± SD @ 10 μM (%)	*eq*BChE inhibition ± SD @ 10 μM (%)	*ee*AChE IC_{50} ± SD (μM)	*eq*BChE IC_{50} ± SD (μM)
5IIh [46]	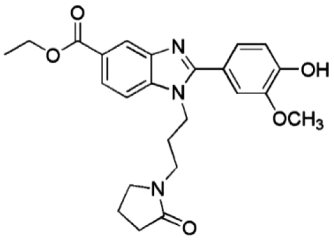	19.54 ± 1.41	35.69 ± 1.74	-	-
5IIi [46]	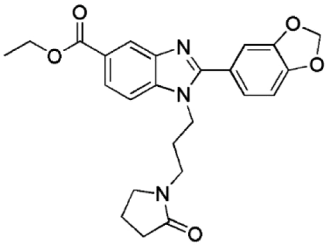	13.24 ± 4.04	44.22 ± 1.68	-	-
5IIj [46]	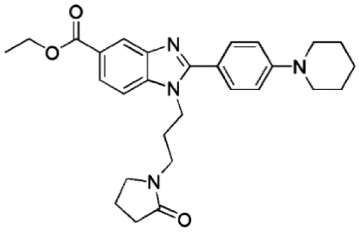	9.04 ± 1.53	48.81 ± 2.88	-	-
5IIk [46]	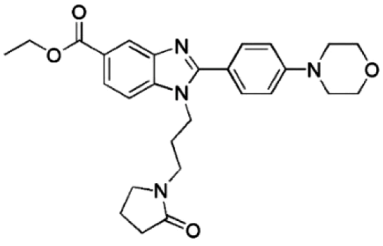	24.26 ± 3.88	11.24 ± 3.90	-	-
5III [46]	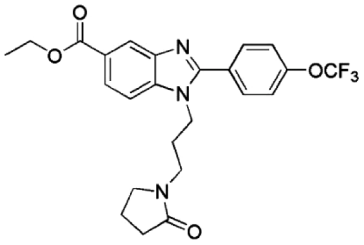	15.19 ± 0.08	50.99 ± 0.72	-	-
Donepezil (10 μM)	-	85.12 ± 4.57	-	0.18 ± 0.08	-
Galantamine (20 μM)	-	-	66.10 ± 4.01	-	4.54 ± 1.26

weaker inhibition, suggesting that substitution at the 6-position of benzimidazole enhances *eq*BChE activity. Larger ester/amide derivatives (**5IIa3, 5IIa4, 5IIa5**, and **5IIa6**) induce a slight decrease in IC_{50}, probably due to steric hindrance, but the main binding mode should not be affected, as illustrated in the crystal structure. Although less potent than tacrine, the control ChE inhibitor, all synthesized derivatives exhibited higher selectivity for *eq*BChE over *ee*AChE (Table 3). This preference likely reflects structural differences between the enzymes: *eq*BChE has a wider catalytic gorge due to the replacement of six of the 14 aromatic residues in *ee*AChE with smaller aliphatic residues, allowing bulkier ligands to bind more effectively [57] Compounds **5IIa1–7** were then tested for their inhibitory activity against *h*BChE (Table 4).

Interestingly, compounds highly potent against *eq*BChE, such as **5IIa1** and **5IIa2**, showed poor inhibition of *h*BChE at 10 μM (Table 4). Only **5IIa5** and **5IIa6** inhibited *h*BChE by >50 %. IC_{50} values were subsequently determined for **5IIa5, 5IIa6,** and **5IIa2** (most potent against *eq*BChE). Among these, **5IIa6** showed the highest potency (IC_{50} = 5.9 μM), while **5IIa5** was weaker, and **5IIa2** was the least active (IC_{50} = 267.76 μM). The improved activity of **5IIa5** and **5IIa6** suggests that incorporation of bulky ring substituents enhances *h*BChE binding, likely through π–π or hydrophobic interactions within the enzyme's active gorge. Binding discrepancies between *h*BChE and *eq*BChE have already been previously reported [49–51], and the potential new π–π

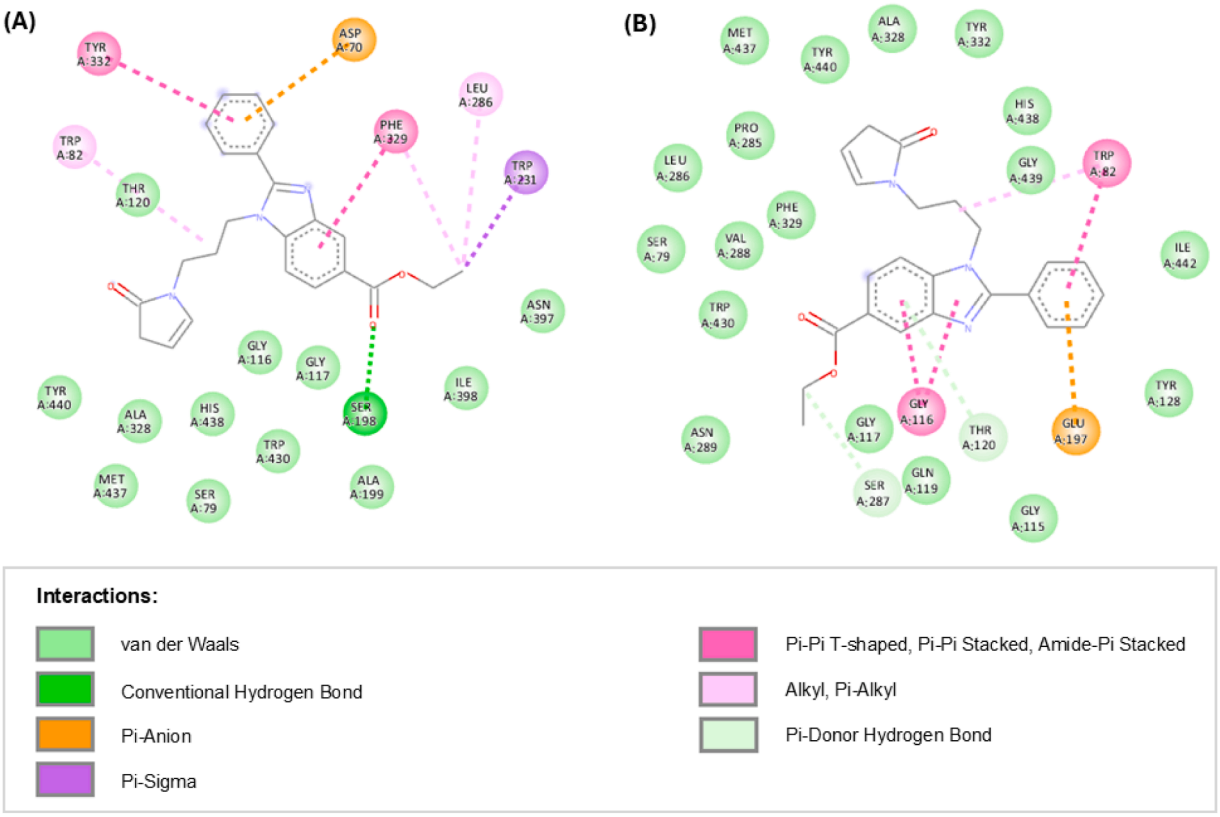

Fig. 3. 2D binding poses of compound 5IIa docked into the active sites of (A) *eq*BChE and (B) *h*BChE. Key ligand–protein interactions are shown and color-coded as indicated.

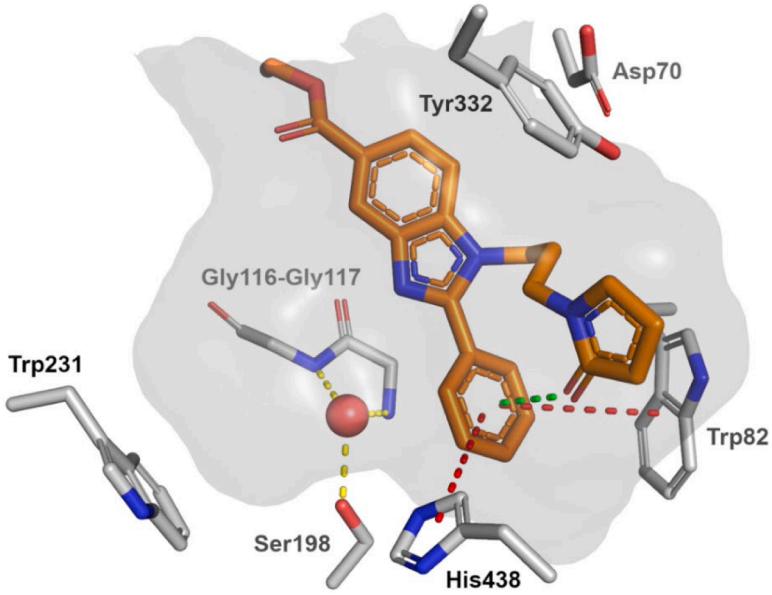

Fig. 4. Illustration of the X-ray *h*BChE-5IIa complex structure. Key residues and compound **5IIa** are represented as sticks, with protein carbon atoms in grey, while **5IIa** carbon atoms are represented in orange. Oxygen and nitrogen atoms are represented in red and blue, respectively. The water molecule present in the oxyanion hole is presented as a red sphere. The transparent grey shade represents the *h*BChE binding pocket. Interactions are represented as dashed lines, with H-bonds in yellow, π–π interactions in red, and the intra-molecular interaction in green.

interactions, especially with Trp231, could drive the compound to rearrange and to adopt an entirely new binding mode. Such behavior could be possible as BChE presents a large active site, with three main possible aromatic interaction sites (Trp231, Trp82, and Tyr332) [58]

2.6. Binding mode

The most potent compound (**5IIa6**) was further investigated through enzyme kinetics. Lineweaver–Burk (LB) plot (Fig. 7) revealed a decrease in maximum velocity (V_{max}) and an increase in Michaelis-Menten

Table 2
Data collection and refinement statistics. Data collection and refinement statistics of *h*BChE in complex with **5IIa**, table calculated using Phenix. R-work = Σ $|F_o - |F_c|| / \Sigma | F_o |$, where F_o and F_c are observed and calculated structure factors, respectively. The R-free set uses about 5 % of randomly chosen reflections. Statistics for the highest-resolution shell are shown in parentheses.

	*h*BChE-5IIa (PDB ID: 9SPC)
Data Collection	
X-ray source	SOLEIL Proxima-2A
Wavelength (Å)	0.9801
Resolution range (Å)	48.74 - 2.66 (2.78 - 2.66)
Space group	I 4 2 2
Unit cell (Å,°)	154.134 154.134 128.387 90 90 90
Total reflections	378,609 (43,358)
Unique reflections	22,436 (2694)
Multiplicity	16.9 (16.1)
Completeness (%)	99.68 (97.61)
Mean $I/\sigma(I)$	11.77 (2.42)
Wilson B-factor (Å[2])	51.94
R-merge	0.1652 (1.122)
R-meas	0.1703 (1.158)
R-pim	0.04106 (0.2837)
$CC_{1/2}$	0.997 (0.749)
CC*	0.999 (0.925)
Refinement statistics	
Reflections used in refinement	22,426 (2690)
Reflections used for R-free	1140 (141)
R-work	0.1799 (0.2743)
R-free	0.2399 (0.3875)
Number of non-hydrogen atoms	4612
macromolecules	4237
ligands	245
solvent	130
Protein residues	526
RMS(bonds)	0.007
RMS(angles)	1.00
Ramachandran favored (%)	95.04
Ramachandran allowed (%)	4.96
Ramachandran outliers (%)	0.00
Rotamer outliers (%)	1.75
Clashscore	4.77
Average B-factor	57.24
macromolecules	55.19
ligands	95.05
solvent	52.57

constant (K_m) with increasing inhibitor concentrations, consistent with a mixed-mode inhibition profile (Table 5). This indicates that **5IIa6** can bind both to the free enzyme (at the acylation site, competitively) and to the enzyme–substrate complex (at the peripheral anionic aromatic site, uncompetitively). Competitive binding blocks access of ACh to the catalytic site, whereas allosteric binding alters enzyme conformation to reduce substrate affinity [59,60]

Mixed-mode inhibition is advantageous over purely competitive inhibition because the inhibitor can prevent ACh hydrolysis regardless of substrate occupancy. From secondary LB plots (Fig. 8 and 9), the inhibition constants K_i and K_{is} were determined as 2.05 μM and 3.02 μM, respectively. The lower K_i value indicates that **5IIa6** has a stronger affinity for free BChE than for the enzyme–substrate complex, further supporting its dual binding capacity [59,60]

2.7. Predicted blood-brain barrier permeability

The BBB is formed by endothelial cells joined by tight junctions, which restrict paracellular diffusion and significantly limit central nervous system (CNS) drug delivery. Consequently, many candidate neurotherapeutics with promising *in vitro* activity fail in clinical trials due to insufficient BBB penetration [61] Therefore, **5IIa6** was tested using the Corning Gentest™ Precoated PAMPA Plate System, a validated model for predicting passive diffusion across the BBB [62,63]

As summarized in Table 6, the effective permeability (P_e) of the lead candidate **5IIa6** was 1.446 × 10^{-5} cm/s, comparable to that of the reference drug donepezil. Based on PAMPA classification, compounds with P_e × 10^{-6} cm/s are considered to have high BBB permeability (CNS+), while those with P_e × 10^{-6} cm/s are classified as CNS- [64] Accordingly, **5IIa6** is predicted to exhibit high BBB permeability. This result is consistent with the high lipophilicity generally associated with benzimidazole derivatives, a physicochemical property favorable for CNS penetration [65]

2.8. Cytotoxicity

The neurotoxicity of **5IIa6** was assessed in neuroblastoma (SH-SY5Y) and microglial (BV2) cells. At 50 μM, **5IIa6**-treated cells remained highly viable, indicating negligible cytotoxicity at the tested concentration (Fig. 10).

3. Conclusion

Two series of benzimidazole derivatives were screened for *ee*AChE and *eq*BChE inhibition, and it was found that 1-propyl-2-pyrrolidinone at the 3-position and unsubstituted phenyl at the 2-position of the benzimidazole nucleus are important for *eq*BChE inhibition. Ethyl 1-(3-(2-oxopyrrolidin-1-yl)propyl)-2-phenyl-1*H*-benzo[*d*]imidazole-5-carboxylate, **5IIa**, stood out with a sub-micromolar *eq*BChE IC_{50} of 0.40 μM and *eq*BChE selectivity index of 14. However, it only moderately inhibits *h*BChE. The X-ray structure of the **5IIa**-*h*BChE complex was determined and displays limited contacts of **5IIa** into the enzyme active site gorge. Based on co-crystallization data with *h*BChE, **5IIa** was structurally modified to yield seven new compounds with high *eq*BChE potency and selectivity. Lead compound **5IIa6** exhibited potency for *h*BChE (5.9 μM), as a mixed-mode inhibitor, with dissociation constants of 3.02 μM (K_{is}) and 2.05 μM (K_i). Importantly, it also displayed high predicted BBB permeability and excellent cellular tolerability in SH-SY5Y and BV2 cells. Collectively, these findings highlight **5IIa6** as a promising benzimidazole-based scaffold for further development as a selective BChE inhibitor in AD therapy. Future studies will focus on comprehensive pharmacokinetic profiling, including metabolic stability, plasma protein binding, *in vitro* cytochrome P450 inhibition, and serum stability, to further support its translational potential.

4. Materials and methods

4.1. Materials

All chemicals and reagents used in the synthesis of benzimidazoles were supplied by Sigma-Aldrich, Merck Chemicals (Germany), Acros Organics and Nacalai Tesque, whereas the solvent used were supplied by J-Kollin, Fisher Chemical and Friendemann Schmidt. Completion of reaction and purity of compounds were checked using thin-layer chromatography (TLC). The solvent systems used as the mobile phase were chloroform-methanol (9:1) or ethyl acetate-hexane (1:4). TLC spots were visualized under short and long UV lights at 254 nm and 365 nm respectively. Synthesized compounds were purified by column chromatography in chloroform: methanol (9:1) solvent system, before validating their structures via ^{1}H NMR, ^{13}C NMR, FTIR and LC-MS. NMR was performed using the Bruker Avance 300 spectrometer at 300 MHz operated by School of Pharmacy. The samples were prepared in either deuterated methanol (MeOD) or chloroform ($CDCl_3$). FTIR was performed using PerkinElmer Spectrum Two™ spectrometer while LCMS was performed on Waters® Xeno™ tQ mass spectrometer by School of Science in positive ESI mode. LCMS samples were prepared in high-performance liquid chromatography (HPLC) grade methanol and filtered using a nylon filter with 0.22 μm pore size.

4.1.1. General procedure for the preparation of benzimidazoles

The final benzimidazole compounds were obtained through a 4-step

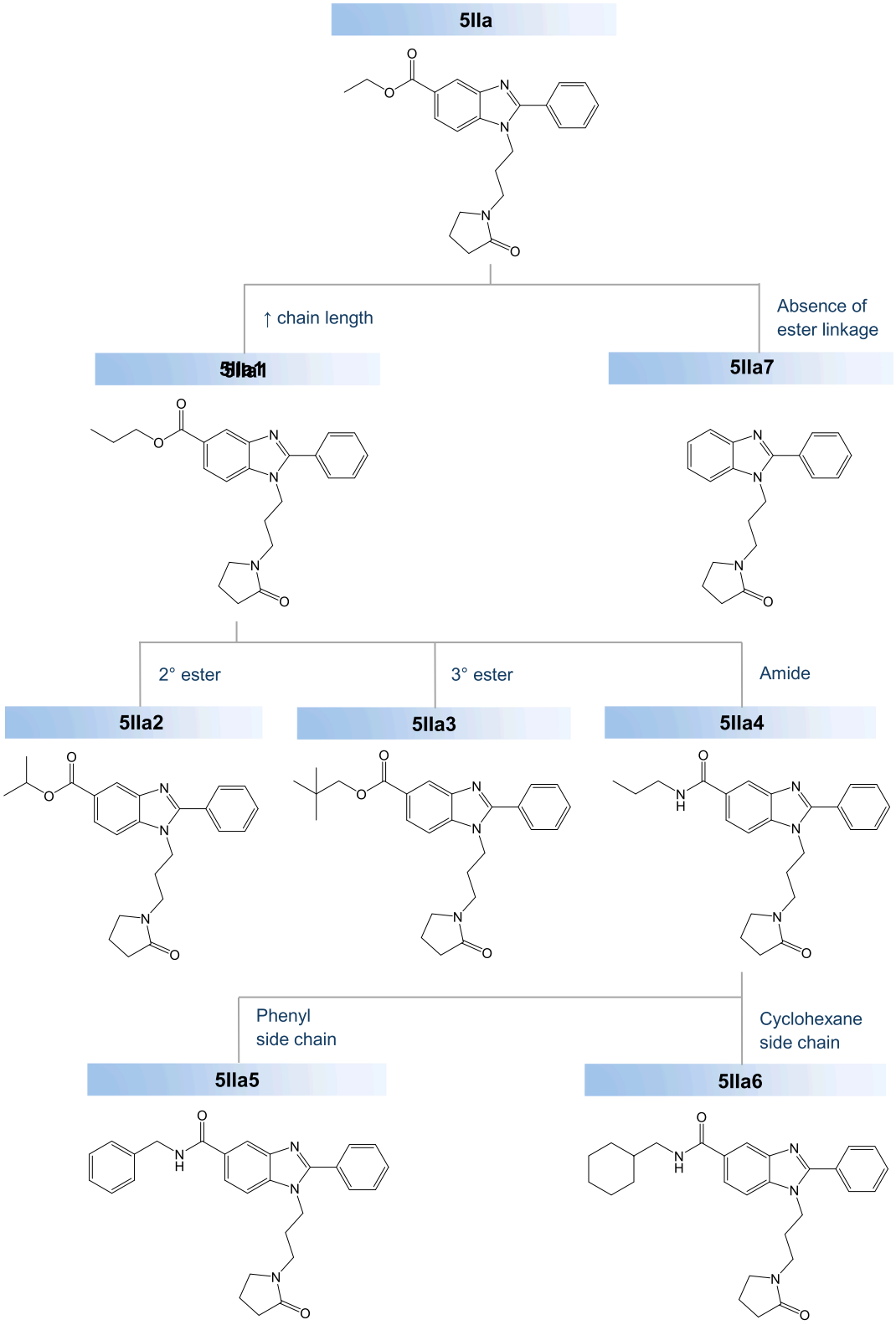

Fig. 5. Structural modification of 5IIa.

synthesis involving esterification, amine alkylation, nitro group reduction, and a final condensation. Sodium bisulfite adducts carrying the desired R^2 moieties were produced on the side *via* a nucleophilic addition. The general protocol was adapted from Yeong et al. [28]

Ethyl-4-fluoro-3-nitrobenzoate (1)

4-Fluoro-3-nitrobenzoic acid (5.4 mmol) was added to ethanol (20 mL) and refluxed for 6 h with acid catalyst, concentrated sulfuric acid (0.4 mL). After cooling down, the reaction mixture was precipitated from cold water. The resultant precipitate was filtered and air dried to give the cream-colored solid product **1** (87 %).

Ethyl-4-(2-substituted amino)-3-nitrobenzoate (2)

Ethyl-4-fluoro-3-nitrobenzoate **1** (1.17 mmol, 1 eq) was dissolved in

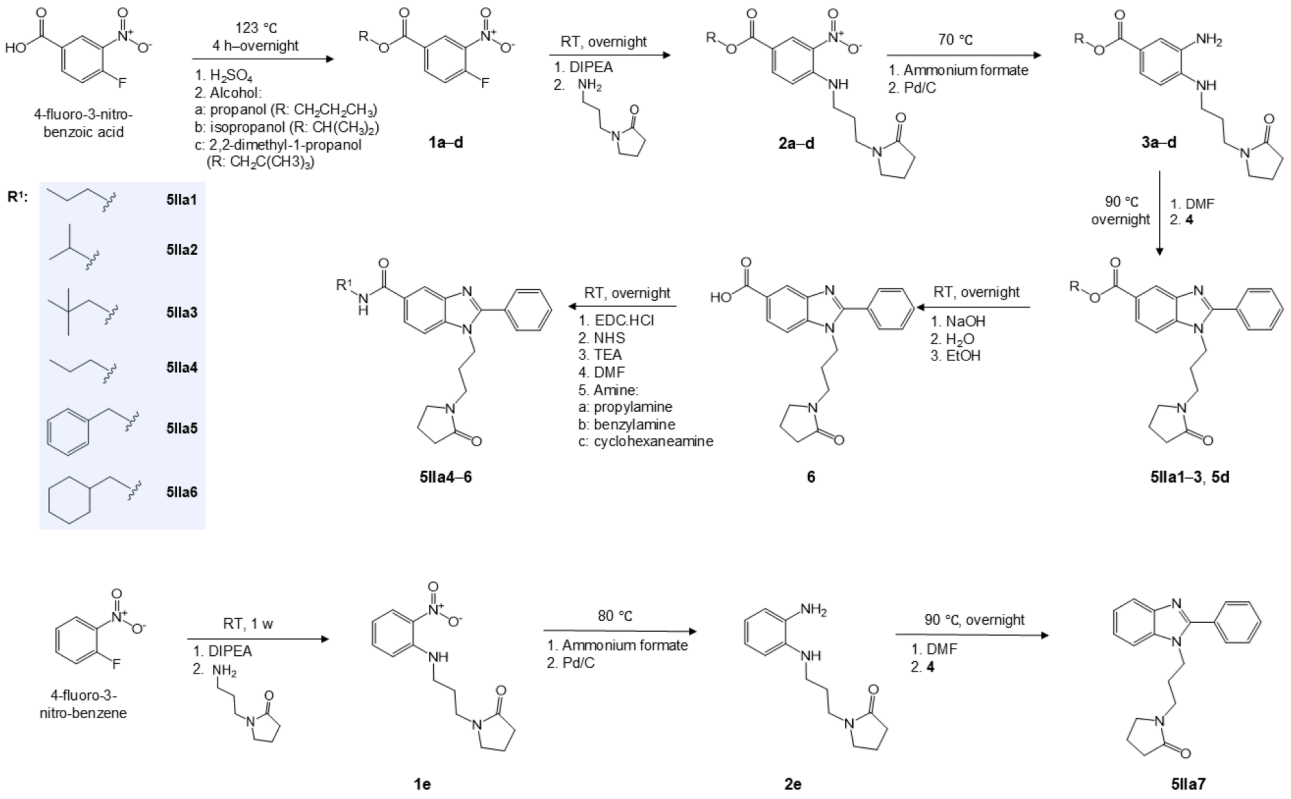

Fig. 6. Reaction pathways for 5IIa modified compounds synthesis.

10 mL of DCM. The amine [**I**: aniline, **II**: *N*-(3-aminopropyl)-2-pyrrolidinone, 1.25 mmol, 1.07 eq] was added into the reaction flask, followed by DIPEA (0.25 mL, 1.44 mmol). Liquid-liquid extraction was performed using 3 × 10 mL distilled water. The organic layer was dried over anhydrous sodium sulfate and evaporated under reduced pressure to yield yellow gel **2** (80–92 %).

Ethyl-3-amino-4-(2-substituted amino)-benzoate (3)

Ethyl-4-(2-subtituted amino)-3-nitrobenzoate **2** (1 mmol, 1 eq) was dissolved in 10 mL of ethanol and heated to 70 °C. Ammonium formate (3.96 mmol, 4 eq) and Pd/C (50 mg) were gradually added into the mixture while stirring. The colour of the reaction mixture was monitored. The reaction was complete when the solution turned from yellow to colourless. The reaction mixture was centrifuged at 2500 g and the supernatant was collected for evaporation under reduced pressure. The product was then re-dissolved in ethyl acetate and washed with 3 × 10 mL distilled water. The organic layer was dried over anhydrous sodium sulfate and evaporated under reduced pressure to yield a yellow liquid **3** (70–85 %).

Sodium bisulfite adducts (4)

The benzaldehyde of interest (5 mmol, 1 eq) was dissolved in 10 mL of ethanol, while sodium metabisulfite (7.5 mmol, 1.5 eq) was dissolved in 3 mL of distilled water. The sodium metabisulfite solution was added dropwise into the reaction mixture over 5 min. The reaction mixture was stirred at room temperature for 2 h and kept overnight at 4 °C. The resultant precipitate was filtered and dried to yield sodium bisulfite adducts **4** (50–95 %).

2-substituted benzimidazole derivatives (5)

For both series, ethyl-3-amino-4-(2-substituted amino)-benzoate **3** (0.6 mmol, 1 eq) and the sodium bisulfite adduct of interest **4** (1 mmol, 1.7 eq) were added to DMF (5 mL) and refluxed at 90 °C overnight. After completion of reaction, 15 mL of ethyl acetate was added to the reaction mixture. Liquid-liquid extraction was performed using 3 × 10 mL distilled water. The organic layer was dried over anhydrous sodium sulfate and evaporated under reduced pressure to yield the final product **5**. In the event of contamination, flash column chromatography was used to purify the final product. The synthesis of **5Ia**–**g** and **5IIa**–**m** were based on published studies [31,46]

4.1.2. General procedure for the preparation of modified benzimidazoles

4-fluoro-3-nitrobenzoate (1a–d)

1a: 4-fluoro-3-nitrobenzoic acid (1.08 mmol), propanol (10 mL) and sulfuric acid (0.15 mL) were refluxed for 4 h at 123 °C. **1b**: 4-fluoro-3-nitrobenzoic acid (2.701 mmol), isopropanol (30 mL) and sulfuric acid (0.5 mL) were refluxed overnight at 123 °C. **1c**: 4-fluoro-3-nitrobenzoic acid (2.161 mmol) was refluxed in 2,2-dimethyl-1-propanol (3 mL) and sulfuric acid (0.1 mL) for 6.5 h at 123 °C. **1d**: 4-fluoro-3-nitrobenzoic acid (8.103 mmol) was left to reflux for 8 h at 123 °C in ethanol (30 mL) and catalytic sulfuric acid (0.6 mL). **1a** and **1b**: Reaction mixture was concentrated under reduced pressure. The crude products were purified via liquid-liquid extraction with DCM and water. The organic layer was collected, dried over sodium sulfate to get rid of any residual moisture and concentrated under reduced pressure to yield **1a** (35 %) and **1b** (62 %) as yellow liquid. **1c** and **1d**: Reaction mixture was added into a beaker of ice to facilitate formation of precipitate. The precipitate formed was filtered using a Büchner funnel to yield **1c** (99 %) and **1d** (87 %).

1-(3-((2-nitrophenyl)amino)propyl)pyrrolidin-2-one (1e)

N,N-Diisopropylethylamine, DIPEA (2.267 mmol, 1.6 eq) and 1-(3-Aminopropyl)-2-pyrrolidinone (1.460 mmol, 1.03 eq) were added to the starting material, 4-fluoro-3-nitrobenzene (0.2 g, 1.417 mmol, 1 eq). The reaction mixture in DCM (15 mL) was stirred for a week at room temperature. Liquid-liquid extraction was then performed using DCM and water. The organic layer was collected, dried over sodium sulfate and concentrated under reduced pressure to yield **1e** (61 %).

3-nitro-4-((3-(2-oxopyrrolidin-1-yl)propyl)amino)benzoate (2a–d)

DIPEA (1.6 eq) and 1-(3-Aminopropyl)-2-pyrrolidinone (1.03 eq) were added to **1a**–**d** (1 eq) in DCM (15 mL). The reaction mixture was

Table 3
IC_{50} of modified benzimidazole compounds at 10 μM against *ee*AChE and *eq*BChE.

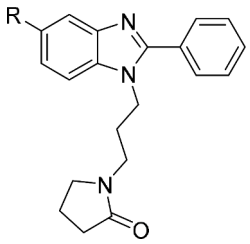

Backbone structure

Compound	R	IC_{50} ± SD (μM)		Selectivity *ee*AChE/*eq*BChE
		*ee*AChE	*eq*BChE	
5IIa1	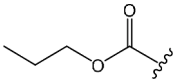	68.15 ± 20.01	1.40 ± 0.07	48.71
5IIa2	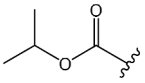	> 100	1.07 ± 0.20	> 93.72
5IIa3	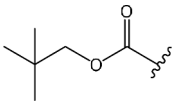	> 100	3.71 ± 0.20	> 26.96
5IIa4	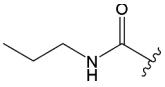	> 100	3.80 ± 0.71	> 26.34
5IIa5	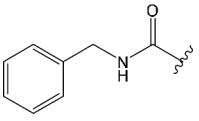	> 100	4.94 ± 0.67	> 20.24
5IIa6	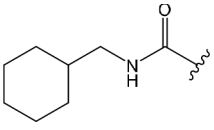	> 100	2.38 ± 0.52	> 42.09
5IIa7		> 100	7.86 ± 0.49	> 12.72
Tacrine (0.05 μM)		0.15 ± 0.01	0.04	3.75
Donepezil (1 μM)		0.22 ± 0.12	6.93 ± 1.48	0.03

Table 4
IC_{50} of modified benzimidazole compounds against *h*BChE.

Compound	*h*BChE inhibition (%) at 10 μM[a]	*h*BChE IC_{50} (μM)
5IIa1	38.63	Nd[a]
5IIa2	31.86	267.76
5IIa3	26.72	Nd
5IIa4	25.51	Nd
5IIa5	53.00	35.59
5IIa6	76.31	5.90
5IIa7	43.16	Nd
Tacrine (0.05 μM)	72.02	0.10

[a] Nd : Not determined.

left to stir overnight at room temperature, then subjected to liquid-liquid extraction with DCM and water. The organic layer was collected, dried over sodium sulfate and concentrated under reduced pressure to yield **2a**–**d** (63–100 %).

1-(3-((2-aminophenyl)amino)propyl)pyrrolin-2-one (2e)

1e (1 eq) was dissolved in ethanol (20 mL) then left to stir at 80 °C while adding in ammonium formate (4 eq) and Pd/C (60 mg). Once the reaction mixture turned colorless, it was centrifuged at 2000 rpm for 5 min. The supernatant was collected and concentrated under reduced pressure. The crude product was redissolved in ethyl acetate to perform liquid-liquid extraction with water. The organic layer was collected, dried over sodium sulfate and concentrated under reduced pressure to yield **2e** (60 %).

3-amino-4-((3-(2-oxopyrrolidin-1-yl)propyl)amino)benzoate (3a–d)

2a–**d** (1 eq) was dissolved in ethanol (20 mL) then left to stir at 70 °C while adding in ammonium formate (4 eq) and Pd/C (40–50 mg). Once the reaction mixture turned colorless, it was centrifuged at 2000 rpm for 5 min. The supernatant was collected and concentrated under reduced

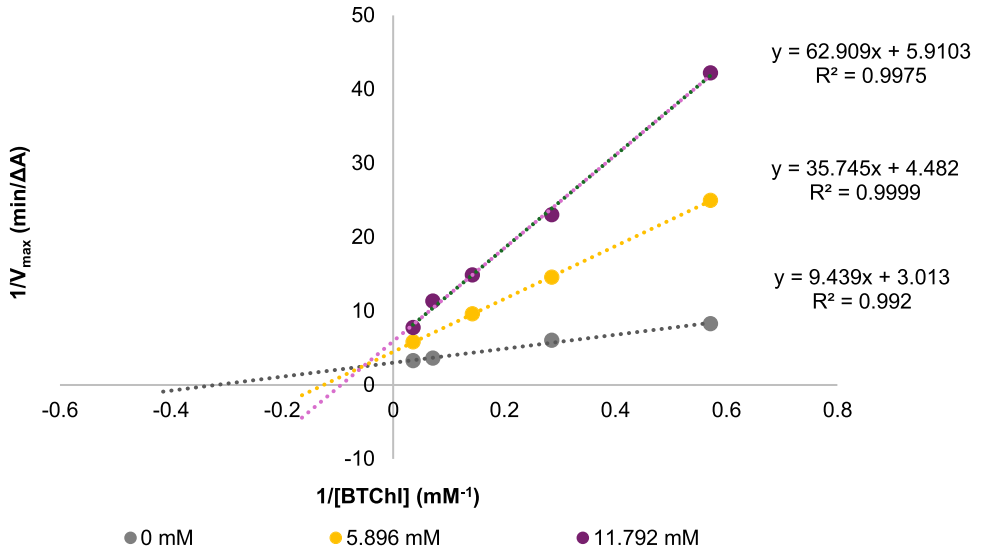

Fig. 7. LB plot of *h*BChE showing the initial velocity at increasing BTChI concentration (1.75, 3.5, 7, 14, 28 mM) in the absence (0 μM) and presence (5.896, 11.792 μM) of **5IIa6**.

Table 5
Kinetic parameters of *h*BChE inhibition by **5IIa6**.

Concentration of 5IIa6 (μM)	V_{max} (mM min^{-1})	K_m (mM)	K_i (μM)	K_{is} (μM)
0	0.33	3.13	2.05	3.02
5.90	0.22	7.98		
11.79	0.17	10.64		

pressure. The crude products were redissolved in ethyl acetate to perform liquid-liquid extraction with water. The organic layer was collected, dried over sodium sulfate and concentrated under reduced pressure to yield **3a**–**d** (53–78 %).

1-(3-(2-phenyl-1*H*-benzo[*d*]imidazole-1-yl)propyl)pyrrolidin-2-one (5IIa7) and 1-(3-(2-oxopyrrolidin-1-yl)propyl)-2-phenyl-1*H*-benzo[*d*]imidazole-5-carboxylate (5IIa1–3, 5d)

A mixture of pre-dissolved **2e** or **3a**–**d** (1 eq) in DMF (5 mL) was added to **4** (1.7 eq). The reaction mixture was refluxed at 90 °C overnight. The crude products were redissolved in ethyl acetate to perform liquid-liquid extraction with water. The organic layer was collected, dried over sodium sulfate, and concentrated under reduced pressure to yield **5IIa7** (from **2e**), **5IIa1**–**3** (from **3a**–**c**), and **5d** (from **3d**).

Propyl 1-(3-(2-oxopyrrolidin-1-yl)propyl)-2-phenyl-1*H*-benzo[*d*]imidazole-5-carboxylate, **5IIa1**. Yield: 87 %; ^{1}H NMR (300 MHz, MeOD): δ (ppm) 1.09 (3H, t, J = 7.2 Hz), 1.82–1.93 (4H, m), 1.95–2.04 (2H, m), 2.27 (2H, t, J = 7.5 Hz), 3.23 (2H, t, J = 6.9 Hz), 3.26 (2H, t, J = 6.9 Hz), 4.31–4.39 (4H, m), 7.64–7.78 (6H, m), 8.08 (1H, dd, J = 0.8 Hz, 8.5 Hz), 8.41 (1H, s). ^{13}C NMR (75 MHz, MeOD): 9.42, 17.31, 21.84, 26.95, 30.41, 39.44, 42.23, 46.93, 66.33, 110.42, 120.55, 124.19, 125.03, 128.77, 129.18, 129.39, 130.36, 138.40, 141.60, 155.57, 166.97, 176.44. IRν_{max} (cm^{-1}): 2921, 1723, 1684, 1499, 1297, 752. LC-MS: m/z 406.0 $[M + H]^+$.

Isopropyl 1-(3-(2-oxopyrrolidin-1-yl)propyl)-2-phenyl-1*H*-benzo[*d*]imidazole-5-carboxylate, **5IIa2**. Yield: 86 %; ^{1}H NMR (300 MHz, MeOD): δ (ppm) 1.42 (6H, d, J = 6.3 Hz), 1.85–1.95 (2H, m), 1.94–2.04 (2H, m), 2.27 (2H, t, J = 7.5 Hz), 3.23 (2H, t, J = 6.6 Hz), 3.26 (2H, t, J = 6.6 Hz), 4.36 (2H, t, J = 7.8 Hz), 5.21–5.33 (1H, m), 7.64–7.78 (6H, m), 8.06 (1H, dd, J = 0.9 Hz, 8.6 Hz), 8.39 (1H, s). ^{13}C NMR (75 MHz, MeOD): 17.31, 20.83, 26.94, 30.40, 39.44, 42.22, 46.93, 68.40, 110.35, 120.50, 124.19, 125.45, 128.77, 129.18, 129.41, 130.36, 138.35,

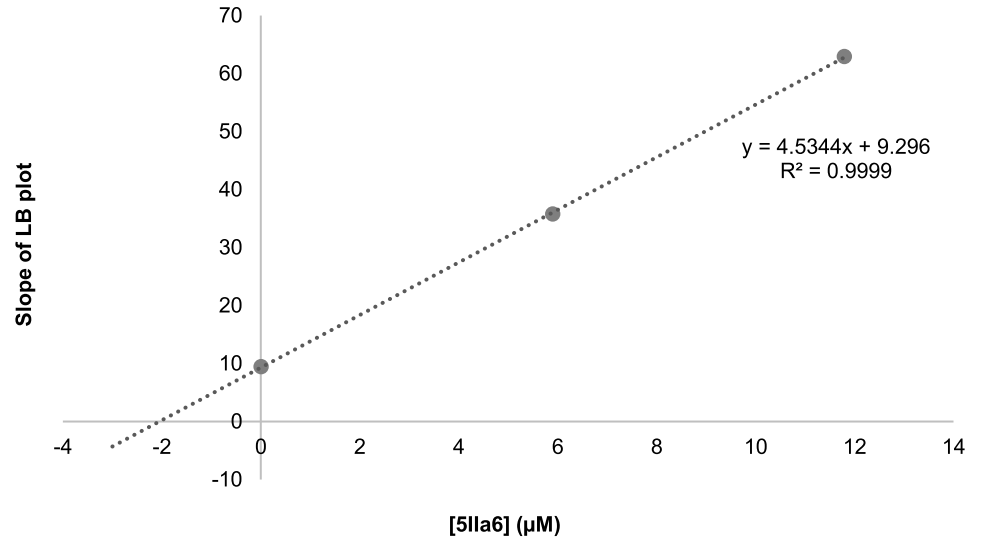

Fig. 8. Secondary plot of slope at increasing **5IIa6** concentration (0, 5.896, 11.792 μM) for the determination of K_i value.

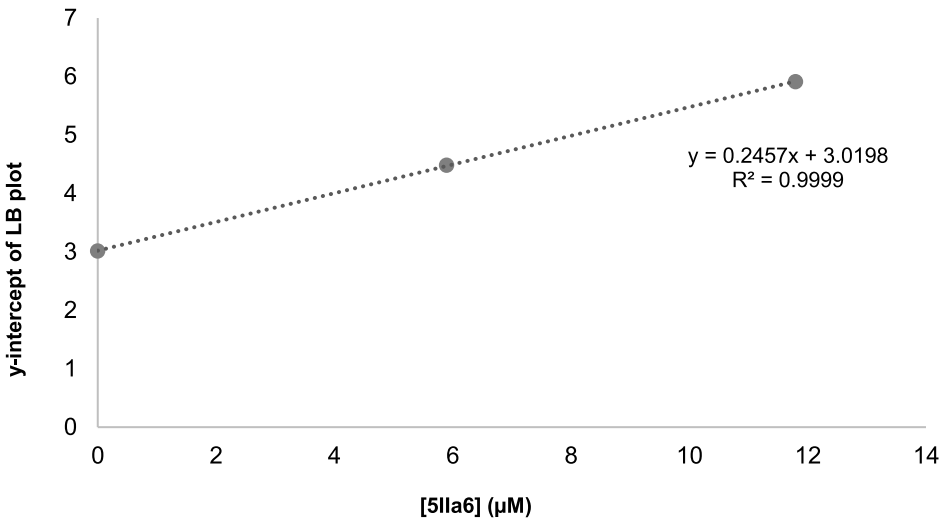

Fig. 9. Secondary plot of y-intercept at increasing **5IIa6** concentration (0, 5.896, 11.792 μM) for the determination of K_{is} value.

Table 6
Effective permeability ($P_e \times 10^{-5}$ cm/s) of **5IIa6** and controls, and their predicted permeability across the BBB into the CNS according to PAMPA classification.

Compound	Effective permeability ± SD ($P_e \times 10^{-5}$ cm/s)	PAMPA classification
5IIIa6	1.45 ± 0.14	CNS+
Caffeine	N[a]	CNS-
Donepezil	1.26 ± 0.08	CNS+

[a] N: no permeability detected at the concentration tested.

141.59, 155.54, 166.44, 176.43. IRν_{max} (cm^{-1}): 2921, 1699, 1682, 1491, 1297, 755. LC-MS: *m/z* 405.9 $[M + H]^+$.

Neopentyl 1-(3-(2-oxopyrrolidin-1-yl)propyl)-2-phenyl-1*H*-benzo[*d*] imidazole-5-carboxylate, **5IIa3**. Yield: 83 %; ^{1}H NMR (300 MHz, MeOD): δ (ppm) 1.10 (9H, s), 1.84–1.94 (2H, m), 1.94–2.04 (2H, m), 2.27 (2H, t, $J = 8.1$ Hz), 3.22 (2H, t, $J = 6.9$ Hz), 3.26 (2H, t, $J = 6.6$ Hz), 4.07 (2H, s), 4.35 (2H, t, $J = 8.1$ Hz), 7.76–7.77 (6H, m), 8.08 (1H, dd, $J = 0.8$ Hz, 8.7 Hz), 8.42 (1H, s). ^{13}C NMR (75 MHz, MeOD): 17.31, 25.55, 26.95, 30.41, 31.17, 39.44, 42.25, 46.94, 73.89, 118.51, 120.53, 124.19, 124.99, 128.78, 129.18, 129.38, 130.37, 138.46, 141.65, 155.62, 166.86, 176.44. IRν_{max} (cm^{-1}): 2950, 1712, 1671, 1492, 1297, 754. LCMS: *m/z* 434.0 $[M + H]^+$.

1-(3-(2-phenyl-1*H*-benzo[*d*]imidazol-1-yl)propyl)pyrrolidin-2-one, **5IIa7**. Yield: 60 %; ^{1}H NMR (300 MHz, $CDCl_3$): δ (ppm) 1.81–1.97 (4H, m), 2.28 (2H, t, $J = 7.8$ Hz), 3.10 (2H, t, $J = 6.6$ Hz), 3.24 (2H, t, $J = 6.9$ Hz), 4.23 (2H, t, $J = 7.8$ Hz), 7.26–7.33 (2H, m), 7.49–7.82 (7H, m). ^{13}C NMR (75 MHz, $CDCl_3$): 17.84, 27.65, 30.79, 39.86, 42.37, 46.87, 109.91, 119.89, 122.76, 123.12, 128.85, 129.30, 130.05, 135.21, 142.50, 153.25, 175.30. IRν_{max} (cm^{-1}): 2920, 1666, 1499, 750. LC-MS: *m/z* 319.9 $[M + H]^+$.

1-(3-(2-oxopyrrolin-1-yl)propyl)-2-phenyl-1*H*-benzo [d] imidazole-5-carboxylic acid (6)

Mixture of sodium hydroxide (6 eq) in water (5 mL) was added dropwise into **5d** (1 eq) in ethanol (10 mL). The reaction mixture was left to stir overnight at room temperature. It was then concentrated at reduced pressure and acidified to pH 3 with hydrochloric acid (HCl). The resulting precipitate formed was filtered to yield **6** (95 %).

1-(3-(2-oxopyrrolin-1-yl)propyl)-2-phenyl-1H-benzo [d] imidazole-5-carboxamide (5IIa4–6)

Triethylamine, TEA (1.5 eq), 1-Ethyl-3-(3-dimethylaminopropyl)carbodiimide hydrochloride, EDC.HCl (1.1 eq), *N*-Hydroxysuccinimide, NHS (1.1 eq) and appropriate amine (1 eq) were added into **6** which was pre-dissolved in DMF (4 mL). The reaction mixture was left to stir overnight at room temperature. After the reaction has completed, sodium carbonate solution (10 % w/v, 5 mL) was added. White solid formed was removed via gravity filtration. Ethyl acetate (20 mL) was then added into the reaction mixture and organic layer was washed with sodium carbonate solution (10 % w/v). Organic layer was then

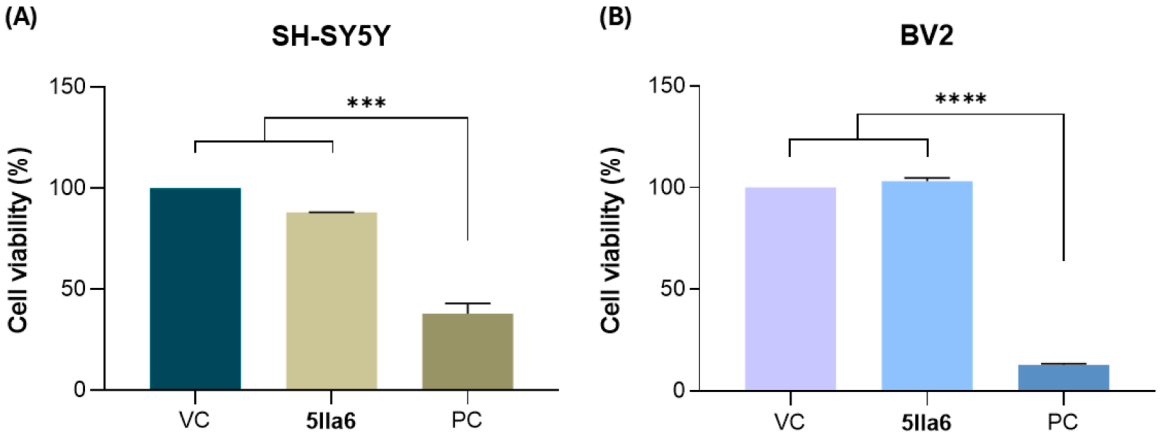

Fig. 10. Viability of (A) SH-SY5Y and (B) BV2 cells upon treatment with 50 μM 5IIa6. VC and PC are vehicle control and positive control, respectively. *** and **** above the error bars indicate *p*-values < 0.001 and < 0.0001, respectively, and statistical difference from PC.

collected, dried over sodium sulfate and concentrated under reduced pressure to yield **5IIa4–6** as brown liquid. Compounds **5IIa4–6** were further purified by column chromatography.

Neopentyl 1-(3-(2-oxopyrrolidin-1-yl)propyl)-2-phenyl-1*H*-benzo[*d*]imidazole-5-carboxylate, **5IIa4**. Yield: 47 %; ^{1}H NMR (300 MHz, MeOD): δ (ppm) 1.02 (3H, t, $J = 7.8$ Hz), 1.63–1.75 (2H, m), 1.84–1.94 (2H, m), 1.94–2.03 (2H, m), 2.27 (2H, t, $J = 7.8$ Hz), 3.22 (2H, t, $J = 6.9$ Hz), 3.25 (2H, t, $J = 6.6$ Hz), 3.40 (2H, t, $J = 7.5$ Hz), 4.34 (2H, t, $J = 7.8$ Hz), 7.63–7.77 (6H, m), 7.89 (1H, dd, $J = 0.8$ Hz, 8.0 Hz), 8.21 (1H, s). ^{13}C NMR (75 MHz, MeOD): 10.42, 17.30, 22.41, 26.94, 30.40, 39.45, 41.52, 42.17, 46.93, 110.37, 117.92, 122.39, 128.75, 129.18, 129.51, 130.28, 137.25, 141.65, 155.27, 168.99, 176.47. IRν_{max} (cm^{-1}): 3378, 2929, 1669, 1638, 1539, 769. LC-MS: *m/z* 404.9 $[M + H]^+$.

N-(cyclohexylmethyl)-1-(3-(2-oxopyrrolidin-1-yl)propyl)-2-phenyl-1*H*-benzo[*d*]imidazole-5-carboxamide, **5IIa5**. Yield: 57 %; ^{1}H NMR (300 MHz, MeOD): δ (ppm) 1.83–1.92 (2H, m), 1.94–2.02 (2H, m), 2.26 (2H, t, $J = 7.8$ Hz), 3.21 (2H, t, $J = 7.2$ Hz), 3.24 (2H, t, $J = 6.9$ Hz), 4.34 (2H, t, $J = 7.8$ Hz), 4.64 (2H, s), 7.28–7.42 (5H, m), 7.63–7.76 (6H, m), 7.93 (1H, dd, $J = 1.1$ Hz, 8.6 Hz), 8.26 (1H, s). ^{13}C NMR (75 MHz, MeOD): 17.29, 26.93, 30.40, 39.44, 42.18, 43.25, 46.92, 110.45, 118.05, 122.51, 126.76, 127.17, 128.14, 127.93, 128.76, 129.17, 129.49, 130.29, 137.38, 139.00, 141.67, 155.32, 168.89, 176.45. IRν_{max} (cm^{-1}): 3284, 2917, 1682, 1645, 1514, 780. LC-MS: *m/z* 452.9 $[M + H]^+$.

N-(cyclohexylmethyl)-1-(3-(2-oxopyrrolidin-1-yl)propyl)-2-phenyl-1*H*-benzo[*d*]imidazole-5-carboxamide, **5IIa6**. Yield: 38 %; ^{1}H NMR (300 MHz, MeOD): δ (ppm) 1.21–1.33 (4H, m), 1.72–1.93 (9H, m), 1.93–2.03 (2H, m), 2.27 (2H, t, $J = 7.5$ Hz), 3.19–3.28 (6H, m), 4.34 (2H, t, $J = 7.8$ Hz), 7.63–7.76 (6H, m), 7.88 (1H, dd, $J = 0.9$ Hz, 8.9 Hz), 8.21 (1H, s). ^{13}C NMR (75 MHz, MeOD): 17.30, 25.68, 26.24, 26.95, 30.75, 30.41, 37.95, 39.45, 42.18, 46.04, 46.93, 110.38, 117.93, 122.43, 128.76, 129.51, 129.18, 129.57, 130.28, 137.25, 141.65, 155.24, 169.05, 176.43. IRν_{max} (cm^{-1}): 3353, 2917, 1676, 1640, 1548, 770. LC-MS: *m/z* 459.0 $[M + H]^+$.

4.2. Cholinesterase inhibitory activity

Acetylcholinesterase (AChE, 500 U/mL, from *Electrophorus electricus*), butyrylcholinesterase from equine serum (*eq*BChE, 1000 U/mL), 5,5'-dithiobis(2-nitrobenzoic acid) (DTNB), acetylthiocholine iodide (ATChI), and butyrylthiocholine chloride (BTChI) were purchased from Sigma-Aldrich. BChE, originating from human serum (*h*BChE, 100 U/mL), was supplied by Creative Enzymes. Positive controls, donepezil and tacrine hydrochloride were purchased from Cayman Chemical Company, while the salts used to prepare 0.1 M phosphate-buffered saline (PBS, pH 7.8) were supplied by Merck and Friendemann Schmidt. ChE inhibitory activity of the test samples was determined by Ellman's microplate assay with modifications [66]

In the AChE inhibitory assay, 140 μL of 0.1 M PBS was added to each well of the clear 96-well plate, followed by 20 μL of test compound. Stock solutions of compounds (10 mM) were prepared in dimethyl sulfoxide (DMSO), diluted with 0.1 M PBS and DMSO to the desired concentrations. The final concentration of DMSO in each well was maintained at 1 % to avoid any interference on enzyme activity. Addition of *ee*AChE (0.1 U/mL, 20 μL) was quickly followed by 15 min of pre-incubation at room temperature, in the dark. DTNB (10 mM, 10 μL) and ATChI (14 mM, 10 μL) were then added into each well. The reaction mixture was incubated for 30 min at room temperature, in the dark, before the absorbance of the yellow end-product at 412 nm was measured using a Tecan Infinite M200 microplate reader. Blank for the test compounds had 20 μL PBS added into the wells to replace the enzyme. 10 % DMSO and donepezil hydrochloride (1 μM) were used to replace the test compounds as negative and positive controls, respectively. The BChE inhibitory assay followed the same procedures, but with different enzyme and substrate, where *eq*BChE (0.1 U/mL, 20 μL), BTChI (14 mM, 10 μL), and tacrine hydrochloride (0.05 μM, 20 μL) were used. *ee*AChE and *eq*BChE inhibitory assays had four technical replicates and were performed in at least duplicate. The *h*BChE inhibitory assay was only conducted once with four technical replicates. The sample absorbance readings were compared to the negative control (1 % DMSO) for each experiment. A logarithmic graph of inhibition (%) against the final concentration of test compounds (μM) was plotted, and the equation of the curve was used to determine the IC_{50} of each compound.

4.3. Binding mode study

LB analysis was performed on the lead compound, which displayed the highest potency against *h*BChE. The same procedures as the ChE inhibitory assay were carried out, with different concentrations of inhibitors and substrates. Firstly, the assay was run in the absence (0 μM) and presence of compounds at two concentrations (IC_{50} and 2 x IC_{50}). Next, a range of BTChI concentrations (1.75, 3.5, 7, 14, and 28 mM) was used. Reciprocal plot (LB plot) of 1/*velocity* against 1/[*substrate*] was constructed. The type of inhibition and the kinetic parameters, such as V_{max} and K_m, were derived from the LB plot using the Michaelis-Menten equation. K_i and K_{is} values were determined from a secondary (Dixon) plot obtained from the LB plot. Each test was conducted in triplicate.

4.4. Molecular docking comparison study

The **5IIa** binding poses were predicted using Boltz-2 from *the eq*BChE and *h*BChE primary sequences (Uniprot IDs Q9N1N9 and P06276), respectively, devoid of the secretion signal peptide and the C-terminus, similarly to the human BChE crystal structure (1P0I), as FASTA files. The **5IIa** ligand was entered as a SMILES string. Structures were computed on an Apple M2-Max MacBook Pro, and inspected with BIOVIA Discovery Studio 2021.

4.5. X-ray crystallographic study

The *h*BChE crystals were obtained using recombinant *h*BChE produced in Chinese hamster ovary cells as a secreted low-glycosylated form devoid of the C-terminal domain involved in protein tetramerization [67] The enzyme is purified from the culture medium after a BChE-specific chromatographic column (Hupresin®, Chemforase, France), followed by a size exclusion chromatography (Superdex-200, Cytiva, France), similarly as previously described [68] Crystals of *h*BChE were obtained by co-crystallization and the hanging drop vapor diffusion at 293 K and 0.1 M MES pH 6.5, 2.15 M $(NH_4)_2SO_4$ as the crystallization buffer. The *h*BChE-**5IIa** complex was obtained by co-crystallization, using 0.1 M MES pH 6.5, 2.15 M $(NH_4)_2SO_4$, 2 mM **5IIa**, where the compound was initially dissolved in MeOH. Crystals were cryo-protected with an NVH oil solution before flash-freezing in liquid nitrogen.

Crystals were collected at the Proxima 2A beamline of the SOLEIL Synchrotron (Saint Aubin, France). Images were auto-processed with autoPROC[69] based on XDS/XSCALE and POINTLESS/AIMLESS software. The initial model was obtained by molecular replacement with the *h*BChE X-ray structure (PDB ID: 1P0I), without ligands, glycans, or water molecules, using the Phaser program in the Phenix software suite [70] The final structure was obtained after iterative cycles of model building using *Coot*[71] and refinement using Phenix.refine. The ligand geometry restraints were calculated using Phenix eLBOW[72] and the semi-empirical quantum-mechanical method (AM1). The structure of *h*BChE in complex with **5IIa** is available in the Protein Data Bank (PDB) under accession number 9SPC. The structure illustration was realized with the PyMOL software (Schrödinger Inc.)

4.6. Prediction of blood-brain barrier permeability

DMSO used for the preparation of stock solutions of compounds (10 mM) was supplied by Macron Chemicals, while salts for PBS were

supplied by Rankem and Merck. Caffeic acid (negative control) and donepezil hydrochloride (positive control) were purchased from Sigma-Aldrich and Nacalai Tesque, respectively. Corning Gentest™ pre-coated PAMPA plate was left to warm to room temperature for 45 min. 0.1 M PBS (200 μL) was added into the acceptor wells, followed by test compounds (200 μM, 300 μL), caffeine (100 μM, 300 μL) and donepezil (200 μM, 300 μL), into the donor wells. The final DMSO concentration in both plates were maintained at 5 %. Acceptor plate was carefully placed on top of donor plate and incubated for five hours in the dark. Then, the absorbance reading of solutions from donor and acceptor plates were measured using a UV–Vis spectrophotometer (UviLine 9400) at their pre-determined lambda max (λ_{max}). Each experiment had three technical replicates and was performed in duplicate. The effective permeability (P_e) of each test compound across the lipid membrane was calculated according to the formula provided in the Gentest™ protocol.

4.7. Cytotoxicity study

Human neuroblastoma (SH-SY5Y) and mouse-derived microglial (BV2) cell lines were supplied by American Type Culture Collection (ATCC). MTT (3-(4,5-dimethylthiazol-2-yl)-2,5-diphenyltetrazolium bromide) and detachment solution (Accutase) were supplied by Merck, while sterile DMSO was supplied by Nacalai Tesque. Trypan blue, Dulbecco's Modified Eagle Medium (DMEM) powder, penicillin streptomycin (Pen-Strep) and fetal bovine serum (FBS) were supplied by Gibco. The salts for 1× PBS (pH 7.6) were supplied by Rankem and Merck. All reagents, buffer and medium were kept and handled at sterile conditions.

SH-SY5Y cells (2×10^4 cells/well) and BV2 cells (2.5×10^3 cells/well) were seeded in a sterile 96-well plate, and the cells were left to adhere for 24 h in the incubator (37 °C, 5 % CO_2). Medium was aspirated prior to the addition of test compounds (50 μM, 100 μL). Test compounds were prepared in sterile DMSO, and the final concentration of DMSO in each well was maintained at 1 %. 1 % DMSO (100 μL) and 5 % DMSO (100 μL) were used as vehicle and positive controls, respectively, replacing the test compounds. After a 24-hour incubation (37 °C, 5 % CO_2), cells were incubated with MTT (0.5 mg/mL) for four hours in the dark, followed by the replacement of MTT media with DMSO to solubilize the purple formazan crystals. DMSO (100 μL) was also added to an additional column as the blank. Absorbance of purple-colored products was measured at 570 nm using a microplate reader (Tecan Infinite M200). Each experiment had four technical replicates and was performed in at least duplicates.

4.8. Statistical studies

One-way analysis of variance (ANOVA) and Dunnett's multiple comparisons test were performed on GraphPad Prism 8. Levels of significance (α), 0.001 and 0.0001, were indicated by *** and ****, respectively. Descriptive statistics were also generated on GraphPad Prism 8.

Funding sources

CSWL and ZYH were supported by the Monash University Graduate Research Pathway Scholarship. XB was supported by the DGA/SSA BioMedef grant NBC-5-C-2316.

Data availability

Data will be made available on request. Structure factors and coordinates of the *h*BChE-**5IIa** complex are deposited in the PDB under accession number 9SPC.

CRediT authorship contribution statement

Christine Shing Wei Law: Writing – original draft, Investigation, Formal analysis. **Zhe Ying Ha:** Writing – original draft, Investigation, Formal analysis. **Xavier Brazzolotto:** Writing – review & editing, Visualization, Validation, Resources, Investigation, Formal analysis. **Keng Yoon Yeong:** Writing – review & editing, Supervision, Conceptualization.

Declaration of competing interest

The authors declare that they have no known competing financial interests or personal relationships that could have appeared to influence the work reported in this paper.

Acknowledgements

The authors wish to acknowledge the School of Science, Monash University Malaysia for supporting this work. The authors would also like to thank the SOLEIL synchrotron for the provision of synchrotron radiation facility beamtime access and the local contacts at the Proxima-A2 beamline for their support.

Supplementary materials

Supplementary material associated with this article can be found, in the online version, at doi:10.1016/j.molstruc.2026.145611.

References

[1] A.P. Porsteinsson, R.S. Isaacson, S. Knox, M.N. Sabbagh, I. Rubino, Diagnosis of early Alzheimer's Disease: clinical practice in 2021, J. Prev. Alzheimers. Dis. 8 (3) (2021) 371–386.
[2] R. Perneczky, F. Jessen, T. Grimmer, J. Levin, A. Fllöel, O. Peters, L. Froelich, Anti-amyloid antibody therapies in Alzheimer's disease, Brain 146 (3) (2023) 842–849.
[3] Y. Ratan, A. Rajput, S. Maleysm, A. Pareek, V. Jain, A. Pareek, R. Kaur, G. Singh, An insight into cellular and molecular mechanisms underlying the pathogenesis of neurodegeneration in Alzheimer's disease, Biomedicines. 11 (5) (2023) 1398.
[4] A.D. Korczyn, L.T. Grinberg, Is Alzheimer Disease a disease? Nat. Rev. Neurol. 20 (4) (2024) 245–251.
[5] B.M. McGleenon, K.B. Dynan, A.P. Passmore, Acetylcholinesterase inhibitors in Alzheimer's disease, J. Clin. Pharmacol. 48 (4) (1999) 471–480.
[6] Y. Ozkay, U.D. Ozkay, Acetylcholine esterase inhibitory potential of some benzimidazole derivatives, Eur. Int. J. Sci. Technol. 3 (7) (2014) 115–120.
[7] K.L. Lanctôt, N. Herrmann, K.K. Yau, L.R. Khan, B.A. Liu, M.M. LouLou, T. R. Einarson, Efficacy and safety of cholinesterase inhibitors in Alzheimer's Disease: a meta-analysis, Can. Med. Assoc. J. 69 (6) (2003) 557–564.
[8] H. Hampel, M.M. Mesulam, A.C. Cuello, M.R. Farlow, E. Giacobini, G.T. Grossberg, A.S. Khachaturian, A. Vergallo, E. Cavedo, P.J. Snyder, et al., The cholinergic system in the pathophysiology and treatment of Alzheimer's disease, Brain 141 (7) (2018) 1917–1933.
[9] Z.R. Chen, J.B. Huang, S.L. Yang, F.F. Hong, Role of cholinergic signaling in Alzheimer's disease, Molecules. 27 (6) (2022) 1816.
[10] R.S. Madnani, Alzheimer's Disease: a mini-review for the clinician, Front. Neurol. 14 (9) (2023) 1178588.
[11] B.R. Williams, A. Nazarians, M.A. Gill, A review of Rivastigmine: a reversible cholinesterase inhibitor, Clin. Ther. 25 (6) (2003) 1634–1653.
[12] Z.Q. Yang, Y. Zou, L.F. Wang, Neurotransmitters in prevention and treatment of Alzheimer's disease, Int. J. Mol. Sci. 24 (4) (2023) 3841.
[13] M. Nasb, W. Tao, N. Chen, Alzheimer's Disease puzzle: delving into pathogenesis hypotheses, Aging Dis. 15 (1) (2024) 43–73.
[14] C.G. Ballard, N.H. Greig, A.L. Guillozet-Bongaarts, A. Enz, S. Darvesh, Cholinesterase: roles in the brain during health and disease, Curr. Alzheimer. Res. 2 (3) (2005) 307–318.
[15] S. Darvesh, G.A. Reid, E. Martin, Biochemical and histochemical comparison of cholinesterases in normal and Alzheimer brain tissues, Curr. Alzheimer. Res. 7 (5) (2010) 386–400.
[16] C. Tan, J. Yu, H. Wang, M. Tan, X. Meng, C. Wang, T. Jiang, X. Zhu, L. Tan, Efficacy and safety,of Donepezil, Galantamine, Rivastigmine, and Memantine for the treatment of Alzheimer's Disease: a systematic review and meta-analysis, J. Alzheimer's Dis. 41 (2) (2014) 615–631.
[17] Z. Breijyeh, R. Karaman, Comprehensive review on Alzheimer's Disease: causes and treatment, Molecules. 25 (24) (2020) 5789.
[18] K.G. Yiannopoulou, S.G. Papageorgiou, Current and future treatments in Alzheimer Disease: an update, J. Cent. Nerv. Syst. Dis. 12 (2020) 1179573520907397.
[19] S. Sadeghian, R. Razmi, S. Khabnadideh, M. Khoshneviszadeh, P. Mardaneh, A. Talashan, A. Pirouti, F. Khebre, Z. Zahmatkesh, Z. Rezaei, Synthesis, biological

evaluation, molecular docking, and MD simulation of novel 2,4-disubstituted quinazoline derivatives as selective butyrylcholinesterase inhibitors and antioxidant agents, Sci. Rep. 14 (2024) 15577.
[20] V. Kumar, N.B. Durai, T. Jobe, Pharmacologic management of Alzheimer's disease, Clin. Geriatr. Med 14 (1) (1998) 129–146.
[21] D.G. Wilkinson, P.T. Francis, E. Schwam, J. Payne-Parrish, Cholinesterase inhibitors used in the treatment of Alzheimer's Disease: the relationship between pharmacological effects and clinical efficacy, Drugs Aging 21 (7) (2004) 453–478.
[22] P. Raina, P. Santaguida, A. Ismaila, C. Patterson, D. Cowan, M. Levine, L. Booker, M. Oremus, Effectiveness of cholinesterase inhibitors and memantine for treating dementia: evidence review for a clinical practice guideline, Ann. Intern. Med 148 (5) (2008) 379–397.
[23] G.T. Grossberg, Cholinesterase inhibitors for the treatment of Alzheimer's Disease: getting on and staying on, Curr. Ther. Res. Clin. Exp. 64 (4) (2003) 216–235.
[24] Z.Y. Ha, S. Mathew, K.Y. Yeong, Butyrylcholinesterase: a multifaceted pharmacological target and tool, Curr. Protein Pept. Sci 21 (1) (2020) 99–109.
[25] N.H. Greig, T. Utsuki, Q.S. Yu, X. Zhu, H.W. Holloway, T. Perry, B. Lee, D. K. Ingram, D.K. Lahiri, A new therapeutic target in Alzheimer's Disease treatment: attention to butyrylcholinesterase, Curr. Med. Res. Opin. 17 (3) (2001) 159–165.
[26] A.L. Guillozet, J.F. Smiley, D.C. Mash, M.M. Mesulam, Butyrylcholinesterase in the life cycle of amyloid plaques, Ann. Neurol 42 (6) (1997) 909–918.
[27] N.H. Greig, T. Utsuki, D.K. Ingram, Y. Wang, G. Pepeu, C. Scali, Q. Yu, J. Mamczarz, H.W. Holloway, T. Giordano, et al., Selective butyrylcholinesterase inhibition elevates brain acetylcholine, augments learning and lowers Alzheimer β-amyloid peptide in rodent, Proc. Natl. Acad. Sci. U.S.A 102 (47) (2005) 17213–17218.
[28] K.Y. Yeong, A.A. Mohamed, C.W. Ang, S.C. Tan, K.K. Khaw, V. Murugaiyah, H. Osman, V.H. Masand, Synthesis, characterization, and molecular docking analysis of novel benzimidazole derivatives as cholinesterase inhibitors, Bioorg. Chem 49 (2013) 33–39.
[29] K.Y. Yeong, A.A. Mohamed, S.C. Tan, R. Ismail, C.W. Ang, R.S. Kumar, H. Osnan, F. Beevi, Antituberculosis: synthesis and antimycobacterial activity of novel benzimidazole derivatives, Biomed. Res. Int. 2013 (1) (2013) 926309.
[30] K.Y. Yeong, A.A. Mohamed, C.W. Ang, S.C. Tan, H. Osman, K. Parang, A.N. Shirazi, Synthesis and evaluation of novel benzimidazole derivatives as sirtuin inhibitors with antitumor activities, Bioorg. Med. Chem 22 (2) (2014) 703–710.
[31] K.Y. Yeong, A.A. Mohamed, C.W. Ang, A.N. Shirazi, K. Parang, S.C. Tan, Benzimidazoles as new scaffold of sirtuin inhibitors: green synthesis, *In vitro* studies, molecular docking analysis and evaluation of their anti-cancer properties, Eur. J. Med. Chem. 83 (2014) 448–454.
[32] K.Y. Yeong, H. Osman, S.C. Tan, Potent Sirtuin inhibition with 1,2,5-trisubstituted benzimidazoles, Medchemcomm. 7 (11) (2016) 2094–2099.
[33] K.Y. Yeong, S.C. Tan, Structural modifications of benzimidazoles *via* multi-step synthesis and their impact on sirtuin-inhibitory activity', Arch. Pharm. (Weinh.) 349 (1) (2015) 1–8.
[34] K.Y. Yeong, C.W. Ang, A.A. Mohamed, H. Osman, S.C. Tan, Antituberculosis agents bearing the 1,2-disubstituted benzimidazole scaffold, Med. Chem. Res. (4) (2017) 770–778, vol. no.
[35] Y.J. Tan, Y.T. Lee, K.Y. Yeong, S.H. Petersen, K. Kono, S.C. Tan, C.E. Oon, Anticancer activities of a benzimidazole compound through sirtuin inhibition in colorectal cancer, Future Med. Chem. 10 (17) (2018) 2039–2057.
[36] C.S.W. Law, K.Y. Yeong, Benzimidazoles in drug discovery: a patent review, ChemMedChem. 16 (12) (2021) 1861–1877.
[37] O. Ozturk, F.M. Farouk, L. Ooi, C.S.W. Law, M.T. Muhammed, E. Aki-Yalcin, K. Y. Yeong, Synthesis of novel carboxamide- and carbohydrazide-benzimidazoles as selective butyrylcholinesterase inhibitors, Mol. Divers 26 (5) (2022) 2863–2876.
[38] A.S. Alpan, S. Parlar, L. Carlino, A.H. Tarikogullari, V. Alptuzun, H.S. Gunes, Synthesis, biological activity and molecular modelling studies on 1*H*-benzimidazole derivatives as acetylcholinesterase inhibitors, Bioorg. Med. Chem 21 (17) (2013) 4928–4937.
[39] G. Coban, L. Carlino, A.H. Tarikogullari, S. Parlar, G. Sarikaya, V. Alptuzun, A. S. Alpan, H.S. Gunes, E. Erciyas, 1*H*-Benzimidazole derivatives as butyrylcholinesterase inhibitors: synthesis and molecular modelling studies, Med. Chem. Res. 25 (9) (2016) 2005–2014.
[40] G. Sarikaya, G. Coban, S. Parlar, A.H. Tarikogullari, G. Armagan, M.A. Erdogan, V. Alptuzun, A.S. Alpan, Multifunctional cholinesterase inhibitors for Alzheimer's Disease: synthesis, biological evaluations, and docking studies of *o*/p-propoxyphenylsubstituted-1*H*-benzimidazole derivatives, Arch. Pharm.- Chem. Life Sci. 351 (8) (2018) 1–18.
[41] K. Ozadali-Sari, T. Küçükkılınç, B. Ayazgok, A. Balkan, O. Unsal-Tan, Novel multi-targeted agents for Alzheimer's Disease: synthesis, biological evaluation, and molecular modeling of Novel 2-[4-(4-Substitutedpiperazin-1-yl)phenyl] benzimidazoles, Bioorg. Chem 72 (2017) (2017) 208–214.
[42] D. Dolles, M. Hoffmann, S. Gunesch, O. Marinelli, J. Möller, G. Santoni, A. Chatonnet, M.J. Lohse, H. Wittmann, A. Strasser, et al., Structure-activity relationship and computational investigations into the development of potent and balanced dual-acting butyrylcholinesterase inhibitors and Human cannabinoid receptor 2 ligands with pro-cognitive *In vivo* profiles', J. Med. Chem 61 (4) (2018) 1646–1663.
[43] Z.Y. Ha, H.C. Ong, C.W. Oo, K.Y. Yeong, Synthesis, molecular docking, and biological evaluation of benzimidazole derivatives as selective butyrylcholinesterase inhibitors, Curr. Alzheimer. Res. 17 (2020) 1177–1185.
[44] E.C. Wagner, W.H. Millet, Benzimidazole, Org. Synth. 19 (12) (1939) 12.
[45] S.I. Alaqeel, Synthetic approaches to benzimidazoles from *o*-phenylenediamine: a literature review', J. Saudi Chem. Soc. 21 (2) (2017) 229–237.
[46] K.Y. Yeong, A.A. Mohamed, C.W. Ang, S.C. Tan, R. Ismail, Synthesis and evaluation of antimycobacterial activity of new benzimidazole aminoesters, Eur. J. Med. Chem. 93 (2015) 614–624.
[47] S.Y. Chiou, C.F. Huang, M.T. Hwang, G. Lin, Comparison of active sites of butyrylcholinesterase and acetylcholinesterase based on inhibition by geometric isomers of benzene-di-*N*-substituted carbamates', J. Biochem. Mol. Toxicol 23 (5) (2009) 303–308.
[48] S. Passaro, G. Corso, J. Wohlwend, M. Reveiz, S. Thaler, V.R. Somnath, N. Getz, T. Portnoi, J. Roy, H. Stark, et al., Boltz-2: towards accurate and efficient binding affinity prediction, bioRxiv (prepr.) (2025).
[49] Chavarria, D, Silva, OD, Benfeito, S, Barreiro, S, Garrido, J, Cagide, F, Soares, P, Remião, F, Brazzolotto, X, Nachon, F et al. 2021, 'Fine-tuning the biological profile of multitarget mitochondriotropic antioxidants for neurodegenerative diseases', *Antioxidants*, vol. 10, no. 2, p. 329.
[50] A. Pasieka, D. Panek, J. Jończyk, J. Godyń, N. Szałaj, G. Latacz, J. Tabor, E. Mezeiova, F. Chantegreil, J. Dias, et al., Discovery of multifunctional Anti-Alzheimer's agents with a unique mechanism of action including inhibition of the enzyme butyrylcholinesterase and γ-aminobutyric acid transporters, Eur. J. Med. Chem. 218 (2021) 113397.
[51] T. Wichur, J. Godyń, I. Góral, G. Latacz, A. Bucki, A. Siwek, M. Głuch-Lutwin, B. Mordyl, J. Śniecikowska, M. Walczak, et al., Development and crystallography-aided SAR studies of multifunctional BuChE inhibitors and 5-HT6R antagonists with β-amyloid anti-aggregation properties', Eur. J. Med. Chem. 225 (2021) 113792.
[52] E. Radzyminska-Lenarcik, K. Witt, The influence of alkyl chain length and steric effect on the stability constants and extractability of Co(II) complexes with 1-alkyl-2-methylimidazoles, Sep. Sci. Technol. 50 (5) (2015) 676–682.
[53] T.N. Thompson, Optimization of metabolic stability as a goal of modern drug design, Med. Res. Rev. 21 (5) (2001) 412–449.
[54] A.E.F. Nassar, A.M. Kamel, C. Clarimont, Improving the decision-making process in the structural modification of drug candidates: enhancing metabolic stability, Drug Discov. Today 9 (23) (2004) 1020–1028.
[55] V. Theodorou, G. Paraskevopoulos, K. Skobridls, A mild alkaline hydrolysis of *N,N*-substituted amides and nitriles, ARKIVOC. 2015 (7) (2015) 101–112.
[56] V. Dragojlovic, Conformational analysis of cycloalkanes, ChemTexts. 1 (14) (2015) 1–30.
[57] F. Pandolfi, D.V. Vita, M. Bortolami, A. Coluccia, R.D. Santo, R. Costi, V. Andrisano, F. Alabiso, C. Bergamini, R. Fato, et al., New pyridine derivatives as inhibitors of acetylcholinesterase and amyloid aggregation, Eur. J. Med. Chem. 141 (2017) 197–210.
[58] T.L. Rosenberry, X. Brazzolotto, I.R. Macdonald, M. Wandhammer, M. Trovaslet-Leroy, S. Darvesh, F. Nachon, Comparison of the binding of reversible inhibitors to Human butyrylcholinesterase and acetylcholinesterase: a crystallographic, kinetic and calorimetric study, Molecules. 22 (12) (2016) 2098.
[59] A. Balkis, K. Tran, Y.Z. Lee, K. Ng, Screening flavonoids for inhibition of acetylcholinesterase identified Baicalein as the most potent inhibitor, J. Agric. Sci. 7 (9) (2015) 26–35.
[60] R.R. Ramsay, K.E. Tipton, Assessment of enzyme inhibition: a review with examples from the development of monoamine oxidase and cholinesterase inhibitory drugs, Molecules. 22 (1192) (2017) 1–46.
[61] K. Tsaioun, M. Bottlaender, A. Mabondzo, ADDME-avoiding drug development mistakes early: central nervous system drug discovery perspective, BMS Neurol. 9 (1) (2009) 1–11.
[62] Y. Zhou, W. Sun, J. Peng, H. Yan, L. Zhang, X. Liu, Z. Zuo, Design, synthesis and biological evaluation of novel copper-chelating acetylcholinesterase inhibitors with pyridine and *N*-benzylpiperidine fragments', Bioorg. Chem 93 (2019) 103322.
[63] A.S. Hogendorf, A. Hogendorf, K. Popiołek-Barczyk, A. Ciechanowska, J. Mika, G. Satała, M. Walczak, G. Latacz, J. Handzlik, K. Kieć-Kononowicz, et al., Fluorinated indole-imidazole conjugates: selective orally bioavailable 5-HT7 receptor low-basicity agonists, potential neuropathic painkillers, Eur. J. Med. Chem. 170 (2019) 261–275.
[64] L. Di, E.H. Kerns, K. Fan, O.J. McConnell, G.T. Carter, High throughput artificial membrane permeability assay for blood-brain barrier, Eur. J. Med. Chem. 38 (2003) 223–232.
[65] C. Sârbu, T. Djaković-Sekulić, N. Perisić-Janjić, Evaluation of lipophilicity of some benzimidazole and benztriazole derivatives by RP HPTLC and PCA, J. Pharm. Biomed. Anal. 30 (3) (2002) 739–745.
[66] G.L. Ellman, A colorimetric method for determining low concentrations of mercaptans, Arch. Biochem. Biophys 74 (2) (1958) 443–450.
[67] F. Nachon, Y. Nicolet, N. Viguié, P. Masson, J.C. Fontecilla-Camps, O. Lockridge, Engineering of a monomeric and low-glycosylated form of Human butyrylcholinesterase, Eur. J. Biochem. 269 (2) (2002) 630–637.
[68] X. Brazzolotto, M. Wandhammer, C. Ronco, M. Trovaslet, L. Jean, O. Lockridge, P. Y. Renard, F. Nachon, Human butyrylcholinesterase produced in insect cells: huprine-based affinity purification and crystal structure, FEBS. J. 279 (16) (2012) 2905–2916.
[69] C. Vonrhein, C. Flensburg, P. Keller, A. Sharff, O. Smart, W. Paciorek, T. Womacka, G. Bricogne, Data processing and analysis with the *autoPROC* toolbox', Acta Crystallogr. D: Biol. Crystallogr. 67 (4) (2011) 293–302.
[70] D. Liebschner, P.V. Afonine, M.L. Baker, G. Bunkóczi, V.B. Chen, T.I. Croll, B. Hintze, L.W. Hung, S. Jain, A.J. McCoy, et al., Macromolecular structure

determination using X-rays, neutrons and electrons: recent developments in phenix, Acta Crystallogr. D: Biol. Crystallogr. 75 (10) (2019) 861–877.
[71] A. Casañal, B. Lohkamp, P. Emsley, Current developments in coot for macromolecular model building of electron cryo-microscopy and crystallographic data, Protein Sci. 29 (4) (2019) 1055–1064.
[72] N.W. Moriarty, R.W. Grosse-Kunstlevea, P.D. Adams, *electronic Ligand Builder and Optimization Workbench* (*eLBOW*): a tool for Ligand coordinate and restraint generation', Acta Crystallogr. D: Biol. Crystallogr. 65 (10) (2009) 1074–1080.